

Chemical Engineering Postgraduate Student Review

Advanced Water Management Centre (AWMC)

Confirmation of PhD Candidature

# Modelling of Purple Phototrophic Bacteria

**Edward Barry**

*Supervisors:*

Damien Batstone

Daniel Puyol Santos

October 19, 2015

## Abstract

Purple phototrophic bacteria (PPB) are an emerging option for wastewater treatment that enables complete recovery of organics and nutrients through assimilation. Although this process appears promising as a new treatment platform, there are several considerations which must be taken into account if it is to be practically implemented. These include characterisation of mixed community activity in a domestic wastewater context. PPB have been studied extensively in the domain of hydrogen production, but the operating conditions cause different metabolic characteristics of the biomass. For example, ammonia has been identified as an inhibitory species for the production of hydrogen, but is always present in wastewater. As the goal of the process is to maximise ammonia and phosphate uptake, these processes are not well understood. Secondly, there has not been analysis into photo-irradiance of mixed culture biomass nor practical implementation into a photobioreactor. There have also been no studies addressing the hydrodynamics of PPB photobioreactors and their implication on reactor performance. Computational fluid dynamics studies have been carried out on algae photobioreactors to assess the flow behaviour of the fluid, and solid biomass particles with different sparging rates and reactor configurations, but these have been greatly simplified to 2 dimensional simulations with basic reactor geometries. Thirdly, the interactions between hydrodynamics, photon delivery and biochemical equations have rarely been successfully implemented in CFD case studies. Finally, there is no understanding of the behavior of pathogens in IR photobioreactor systems, and modelling of pathogens in general in wastewater systems is limited.

Four research objectives have been proposed to advance these current limitations specifically in the context of development of PPB based photo-anaerobic membrane bioreactor (PAnMBR) systems for wastewater treatment. The identified research gaps are as follows;

1. Develop a mechanistic model for applications of PPB for domestic wastewater treatment and apply it for system assessment.
2. Develop a generic stochastic model for pathogen removal in wastewater treatment processes.
3. Quantify the interactions between cell growth and photon availability in order to extend the recently developed photoanaerobic model 1 (PAM1).
4. Optimise the design of the PAnMBR for maximal performance and minimal operating costs (energy expenditure) and capital expenditure.

In terms of progress, objective 1 has been completed and a paper is in draft (Daniel Puyol is principal author). My contribution was continuous process modelling, data collection and analysis, and as key contributor to model development. Data towards objective 2 has been collected, and the model formulation is complete, with the paper ready for drafting. A two dimensional CFD model has been completed for objective 3, and the results from research objectives 1 and 3 will need to be completed before work on objective 4 commences.



## Contents

<b>1</b>	<b>Introduction</b>	<b>1</b>
<b>2</b>	<b>Background and Literature Review</b>	<b>3</b>
2.1	Wastewater Treatment Lumped Parameter Modelling . . . . .	3
2.2	Purple Phototrophic Bacteria Growth Models . . . . .	3
2.3	Phototrophic Bacteria and Irradiance . . . . .	4
2.4	Computational Fluid Dynamics in Wastewater Treatment Modelling . . . . .	6
2.4.1	Bubble Column Models . . . . .	7
2.4.2	Photobioreactor CFD Models . . . . .	8
2.4.3	Bioreactor Design Optimisation Models . . . . .	9
2.5	Pathogen Removal . . . . .	10
2.6	Summary of Research Gaps . . . . .	12
<b>3</b>	<b>Research Objectives</b>	<b>13</b>
3.1	Research Objective 1 . . . . .	13
3.2	Research Objective 2 . . . . .	13
3.3	Research Objective 3 . . . . .	13
3.4	Research Objective 4 . . . . .	13
<b>4</b>	<b>Methodology and Progress to Date</b>	<b>14</b>
4.1	Research Objective 1 . . . . .	14
4.1.1	Materials and Methods . . . . .	14
4.1.2	Achievements to Date . . . . .	14
4.1.3	Conclusions . . . . .	19
4.2	Research Objective 2 . . . . .	19
4.2.1	Materials and Methods . . . . .	19
4.2.2	Achievements to Date . . . . .	21
4.2.3	Expected Outcomes . . . . .	21
4.3	Research Objective 3 . . . . .	22
4.3.1	Materials and Methods . . . . .	22
4.3.2	Achievements to Date . . . . .	23
4.3.3	Expected Outcomes . . . . .	25
4.4	Research Objective 4 . . . . .	26
4.4.1	Materials and Methods . . . . .	26
4.4.2	Expected Outcomes . . . . .	26
4.5	Timeline . . . . .	26
<b>References</b>		<b>27</b>
<b>Appendix A</b>		<b>34</b>



## List of Figures

1	Demonstration of planetary boundaries showing the stable operating space of biochemical flows being surpassed (Steffen et al., 2015) . . . . .	1
2	Model of the LH2 complexes surrounding the LH1-RC complexes for <i>Rhodobacter sphaeroides</i> . Only the B850 units of the LH2 have been included in this representation (Baghbanzadeh and Kassal, 2015) . . . . .	4
3	Cartoon of energy transport mechanisms of light harvesting complexes of Rhodobacterales. Energy transfer is shown by the shaded grey arrows, while the black arrows demonstrate the redox reactions occurring. (Cogdell et al., 2006a) . . . . .	5
4	Petersen matrix summarising rates of all metabolic mechanisms for PAM1 . . . . .	16
5	Dependence of the PAnMBR on initial concentrations of soluble COD and inorganic nitrogen . . . . .	17
6	Effect of dark/light cycles on PPB metabolism under low (double lines) and high (single lines) chemoheterotrophic activity ( $k_{M, ch} = 0.074$ and $0.7 \text{ g COD g}^{-1} \text{ COD d}^{-1}$ , respectively). Simulation of the evolution of acetate (continuous line), ethanol (dashed line), and biomass (dash-dot lines) concentrations during 1 h dark/light periods. . . . .	18
7	Photoautotrophic uptake of inorganic carbon. The blue region shows the literature values simulated 10 000 times. The darker colour denotes a higher probability of inorganic carbon uptake. The mean of the samples is plotted as a thick black line, and the 95% confidence limits are the two bounding dotted lines. The thick dotted line is the value determined in the batch tests with PPB from domestic wastewater. . . . .	19
8	Absorbance spectrum of typical PPB. The purple stars show wavelengths at which carotenoids absorb photons, and the green stars show where bacteriochlorophylls absorb photons (Adessi and De Philippis, 2014) . . . . .	22
9	Initial design by KBR . . . . .	23
10	Two dimensional mesh generated in Salomé . . . . .	24
11	Eddy formation after 10 s of operation . . . . .	25
12	Timeline for PhD work . . . . .	26

## List of Tables

1	Maximum theoretical <i>Rb. capsulatus</i> yield with acetate as electron donor for different wavelengths (Minkevich et al., 2004) . . . . .	6
2	PPB experimental yield for different wavelengths and lactate and acetate as electron donors(Minkevich et al., 2004) . . . . .	6
3	Indicator pathogen quantification methods . . . . .	20
4	Results for the sampling carried out between April 2015 and July 2015. The results have been expressed as average log reductions to a 95% confidence interval.	21



## 1 Introduction

Current domestic wastewater treatment involves the removal of nutrients, metals, organics and pathogens to ensure that environmental and public health impacts downstream are minimised (Tchobanoglou et al., 2003). The scope of wastewater treatment must change in order to cope with the growing global human population (Matassa et al., 2015). The major nutrients contributing to the world food supply are nitrogen in its biologically reactive forms, and phosphorus in the form of phosphate (Verstraete et al., 2009).

The current situation sees nitrogen, the most abundant gas in the atmosphere, being fixed through the Haber Bosch process to form ammonia. This process accounts for roughly 1.5% of the global energy demand. In addition, the nitrogen cycle is being pushed past its safe operating space due to anthropogenic inputs, particularly to agriculture (Steffen et al., 2015).

Much like the nitrogen cycle, the phosphorus cycle is also being driven past its stable operating space (Steffen et al., 2015). Phosphorus rock is being mined at greater rate than itâŽs being naturally deposited. It is expected that global phosphorus demand will surpass supply by 2035 (Cordell et al., 2009). In addition, available phosphate rock is concentrated mostly in North-West Africa. With global demand exceeding supply, and the bulk availability being concentrated in a small region, geopolitical stability could be compromised if actions aren't taken concerning the phosphorus cycle (Cordell et al., 2009). Figure 1 shows by how much the biochemical cycles have passed their stable state.

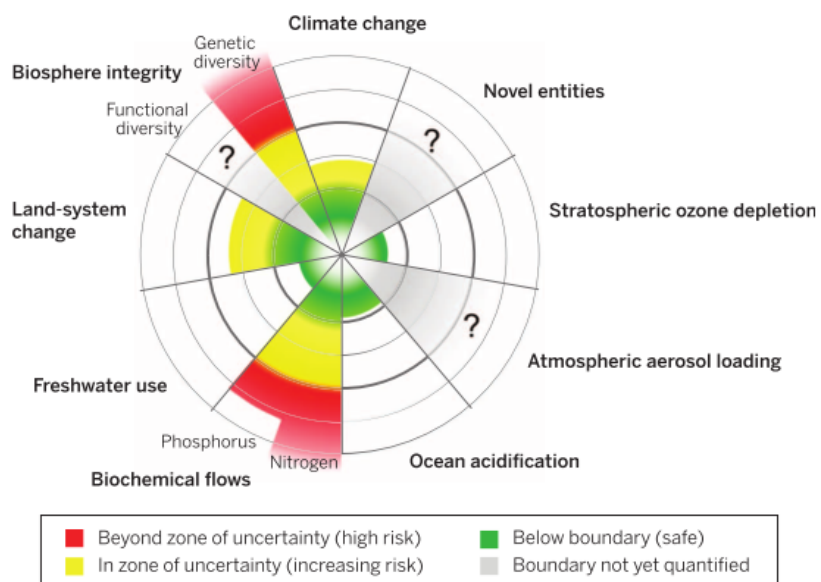


Figure 1: Demonstration of planetary boundaries showing the stable operating space of biochemical flows being surpassed (Steffen et al., 2015)



A number of key studies have advocated reimaging of wastewater treatment towards a resource recovery concept. Verstraete et al. (2009) proposed the idea that, given the contained quantities of organics and nutrients, used wastewater should be seen as a resource, and not as a waste stream. It was in this study that the hypothetical framework of *partition, release, recover* was proposed (Batstone et al., 2015). In contrast, McCarty et al. (2011) proposed a low strength, mainline anaerobic treatment regime of domestic wastewater which would maximise the energy recapture from the organics using anaerobic membrane bioreactors (AnMBR) or upflow anaerobic sludge blanket (UASB) systems. Both concepts were further developed and compared by Batstone et al. (2015) and it was identified that the McCarty concept was more energy efficient, but the *partition-release-recover* concept had a better opportunity for nutrient recovery. The partition step refers to the transfer of organics and nutrients to a solid phase, and is the key component of the process. Hülsen (2015) enriched purple phototrophic bacteria (PPB) and demonstrated that they were able to achieve complete single stage treatment in batch (Hülsen et al., 2014), and in continuous operation (Hülsen et al., 2015) in a photo anaerobic bioreactor (PAnMBR). The system showed that PPB were able to uptake organics, ammonium-N ( $NH_4 - N$ ), and phosphate ( $PO_4 - P$ ) with a ratio of 100 : 8.6 : 1.5 respectively in the presence of near infra-red (NIR) radiation. The major process bottlenecks identified were that VFA-COD were a limiting substrate in a medium strength domestic wastewater which generally has a SCOD:N:P ratio of 100:15:3.5 (Tchobanoglous et al., 2003). Another key issue is that light energy input has not been properly quantified, and is a key issue to minimize capital and operating cost. This challenge formed the major motivation of this research project – the quantification and characterisation of the irradiance required for the PPB to function as intended.

The scope of this project is to develop mechanistic and stochastic models to aid in understanding the underlying processes of the system. A review of several existing modelling techniques in wastewater treatment has been conducted in order to develop an appropriate methodology to modelling the purple phototrophic bacteria system including mechanistic wastewater process modelling, application of distributed parameter models, and the use of a range of laboratory and experimental platforms.

## 2 Background and Literature Review

### 2.1 Wastewater Treatment Lumped Parameter Modelling

Models use mathematical expressions in order to explain or reflect the underlying processes or inputs and outputs of a system (Hangos and Cameron, 2001). Models can be classed according to the method of their development. When developing a wastewater treatment model, one must make decisions which affect the data collection technique, the equations to employ, and the development environment to use. The major binary classes are; mechanistic or empirical models, stochastic or deterministic models, continuous or discrete models and lumped parameter or distributed parameter models (Hangos and Cameron, 2001). In reality, model developers might use a combination of these different categories depending on the target use of the model. This section focusses on the established lumped parameter wastewater treatment (WWT) models, i.e. those describing the dependent variables as a function of time and not space.

The major biological mechanistic generic models in WWT are the International Water Association (IWA) models. These include the activated sludge model (ASM) family, the anaerobic digestion model (ADM) family. These have been combined together with appropriate unit process models such as the Takacs clarifier models (Takacs et al., 1991) into standardized plant wide models such as the benchmark simulation model (BSM) family. Modelling of wastewater treatment processes (WWT) can lead to a greater understanding of the underlying physics and biochemistry (Szilvester et al., 2010). All the IWA models are semi-mechanistic, which means that the model equations are based on known mechanistic phenomena, such as the presence and behavior of known biological clades, but the kinetic relationships (such as Monod or first order) are generally stochastic.

#### *Comments on Applicability of Current IWA Models*

These models are useful in understanding the underlying biochemical processes occurring in wastewater treatment systems. They also serve as good tools for process unit design in wastewater treatment plants. The benefits of these models are that they are readily extensible, and allow themselves to be used in distributed parameter models (Batstone et al., 2006). This also means that the IWA models can be applied for PPB time-series and distributed parameter models for a wastewater treatment context, with possible modification of half saturation parameters particularly.

### 2.2 Purple Phototrophic Bacteria Growth Models

Purple phototrophic bacteria are some of the most metabolically versatile organisms on earth (Hunter et al., 2008). They have been demonstrated to grow well photoheterotrophically under anaerobic conditions (Hülsen et al., 2014). They also grow chemoheterotrophically in the absence of irradiance, and photoautotrophically, using irradiance to drive  $CO_2$  fixation (Gordon and McKinlay, 2014). With respect to modelling of phototrophic bacteria, there currently exist no models of the system in a wastewater treatment con-



text. There are metabolic models relating to developing an understanding of the electron transport chain, but not for particular industrial applications of PPB (Klamt et al., 2002, 2008; Golomysova et al., 2010).

## 2.3 Phototrophic Bacteria and Irradiance

Purple phototrophic bacteria have evolved to efficiently harvest available solar radiation in aquatic environments (Cogdell et al., 2006a). Due to oxygenic photosynthetic organisms filtering visible spectrum radiation in the upper aerobic zones of these aquatic systems, PPB have adapted to make use of remaining wavelengths, which include green and near infrared radiation (Cogdell et al., 2006b). The light harvesting apparatus in Rhodobacterales consists of two light harvesting complexes (LH2 and LH1), and a reaction centre (RC) (Hellingwerf et al., 1994). It is more useful to think of two principal complexes, LH2, and a coupled LH1-RC centre, each of which have primarily bacteriochlorophylls (Bchl)s showing clear absorbance at 800 nm and 850 nm for the LH2 complex, and 880 nm for the LH1-RC complex. As such, the bacteriochlorophylls are commonly referred to as B800, B850 and B880 respectively (Baghbanzadeh and Kassal, 2015). Figure 2 provides a representation of the light harvesting complexes of *Rhodobacter sphaeroides*, which dominated in a wastewater fed system (Hülsen et al., 2014). Figure 3 demonstrates the mechanism by which ATP is generated as a result of the photon harvesting complexes. This schematic is useful to visualise the importance of the light harvesting complexes for cell growth and maintenance, and subsequently, reactor performance.

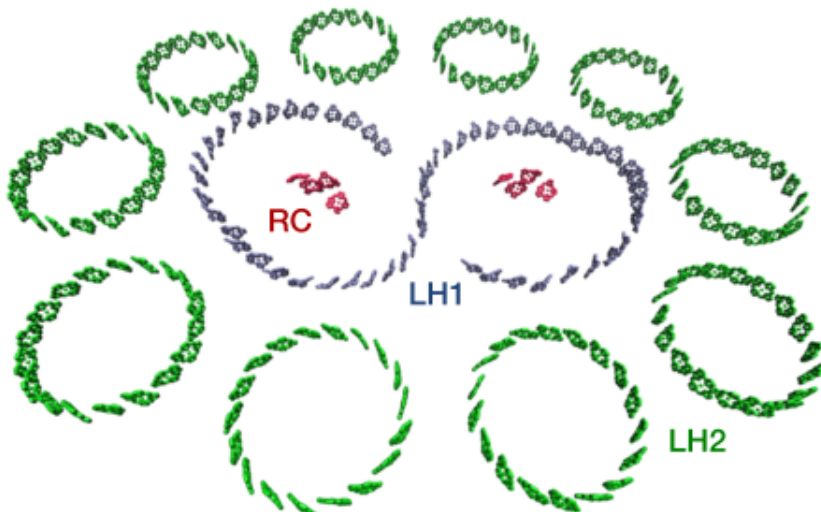


Figure 2: Model of the LH2 complexes surrounding the LH1-RC complexes for *Rhodobacter sphaeroides*. Only the B850 units of the LH2 have been included in this representation (Baghbanzadeh and Kassal, 2015)

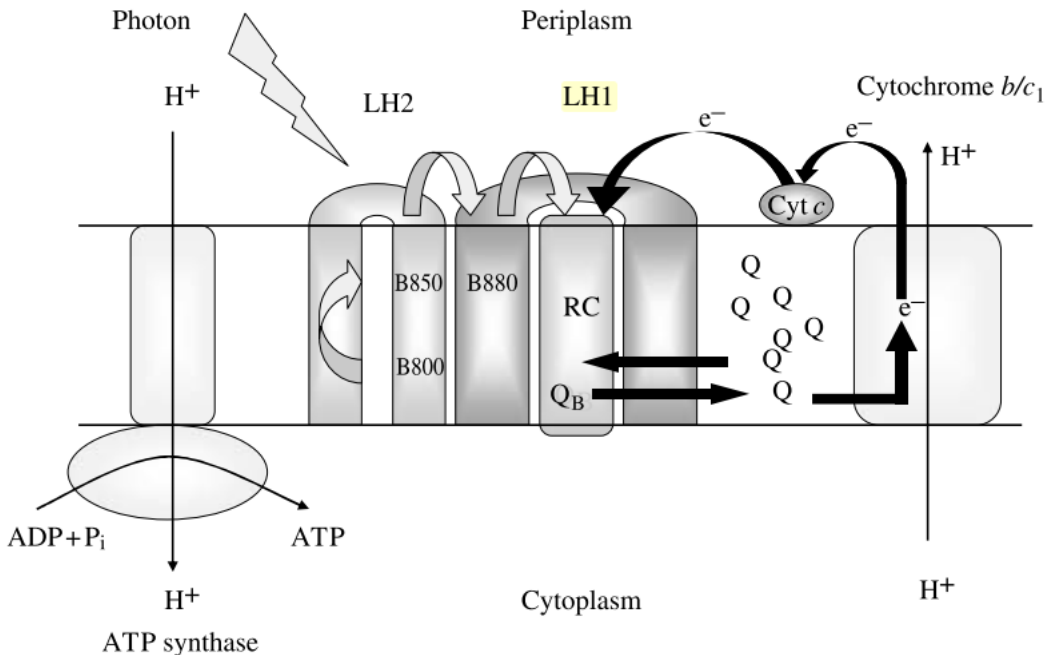


Figure 3: Cartoon of energy transport mechanisms of light harvesting complexes of Rhodobacterales. Energy transfer is shown by the shaded grey arrows, while the black arrows demonstrate the redox reactions occurring. (Cogdell et al., 2006a)

In terms of modelling PPB and their interactions with photons for industrial applications, very little has been done. Most studies focusing on photobioreactor design have been for hydrogen production applications. Adessi and De Philippis (2014), identified all studies were performed using pure cultures of either *Rhodobacter sphaeroides* or *Rhodopseudonomas palustris*. Further limitations to these works were that particular wavelengths were not selected, with most opting for direct sunlight or white tungsten or halogen lamps as light sources. These approaches are problematic for a wastewater treatment application, as the use of broad spectrum light will lead to competition by other heterotrophic bacteria, and other phototrophic and photosynthetic organisms found in domestic wastewater such as algae and cyanobacteria.

Efforts were made to combine a mass balance approach to the photoheterotrophic efficiency of PPB (Minkevich et al., 2004). In this work, theoretical and experimental yields of purple phototrophic bacteria were calculated based on different electron donors and light sources. The maximum theoretical yields based on acetate as an electron donor are summarised in 1, where  $Y_{X/LE}^m$  is the maximum biomass growth per light energy dose;

Table 1: Maximum theoretical *Rb. capsulatus* yield with acetate as electron donor for different wavelengths (Minkevich et al., 2004)

Wavelength	$Y_{X/LE}^m (gVSS \cdot kJ^{-1})$
860 nm	0.020
744 nm	0.017
522 nm	0.012

The theoretical model was then compared to experimental data, with the following values obtained through experiment. This information is presented in Table 2.

Table 2: PPB experimental yield for different wavelengths and lactate and acetate as electron donors(Minkevich et al., 2004)

Species	Wavelength	Electron donor	$Y_{X/LE} (gVSS \cdot kJ^{-1})$
<i>Rb. capsulatus</i>	860 nm	lactate	0.018 - 0.031
<i>Rb. sphaeroides</i>	White ( $\lambda = 744$ nm)	acetate	0.009 - 0.016
<i>Rb. capsulatus</i>	522 nm	lactate	0.006 - 0.013

The data of Minkevich et al. (2004) serves as an effective basis for quantifying and understanding the interactions between biomass growth, maintenance and decay, and the irradiance required for optimal reactor performance.

## 2.4 Computational Fluid Dynamics in Wastewater Treatment Modelling

Traditional design methods of wastewater treatment process units consist of load and mass based static analysis, and limited testing of dynamic behavior based on key operating state variables (Gaden, 2013). Computational fluid dynamics is a cost-effective method for scaling-up process units and testing variations in key operating parameters in order to design equipment without having to physically prototype equipment (Wood et al., 1995). Computational fluid dynamics (CFD) involves the spatio-temporal numerical analysis of transport equations and chemical reactions (Versteeg and Malalasekera, 2007). There have been many applications for CFD, including aerodynamic studies of aircraft, turbine analysis in power plants, environmental modelling of pollutants and biomedical analysis of blood flows (Versteeg and Malalasekera, 2007). The major CFD studies in water treatment modelling have been conducted in the fields of algae growth, the inactivation of pathogens by ultraviolet (UV) radiation, and geometry and flow optimisation of conventional treatment plant units such as clarifiers, ponds and digesters. Although UV disinfection is important, the field is quite far removed from nutrient recovery that it has been omitted from this report. The remaining areas of research have been



chosen as a basis for literature review because the most important factors to consider when designing and scaling-up a photobioreactor are radiation intensity and distribution and gas and liquid and particulate solid flow patterns (Bitog et al., 2011). As such, an analysis of existing bubble column models, photobioreactor models including light delivery, anaerobic digester models incorporating non-newtonian fluids and accounting for dynamic densities, and flow-biokinetic coupled bioreactors has been carried out in order to develop an understanding of the modelling techniques employed, and the limitations of current studies in the literature.

#### 2.4.1 Bubble Column Models

There are numerous studies looking at modelling bubble columns in a spatio-temporal manner. One of the early works in this field identified a need to consider a modelling technique incorporating spatio-temporal variations in order to minimise capital and operating costs during scale-up of general bubble column reactors (Lapin and Luebbert, 1994). In this study, the Navier-Stokes system of equations were modelled in a continuous, and the dispersed gas bubbles were modelled as discrete tracked particles, with their position being solved over time. As this was a 1994 study, the computing power limited the model development to a two dimensional 60 x 200 grid of a  $0.75m^2$  reactor face. Numerical diffusion arose when the a continuous reference frame was used for both liquid and gas phases. With the improvement in desktop computing capacity, CFD has been used extensively for bubble column and airlift reactor validation using both approach (Bitog et al., 2011). Other studies have looked at describing bubble flow within different reactor geometries with Eulerian-Eulerian (both phases considered continuous) methods (Lehr et al., 2002; Pfleger and Becker, 2001; Buwa and Ranade, 2002; Pareek et al., 2003; Ekambara et al., 2005; Sokolichin and Eigenberger, 1999). Gas-liquid flow in bubble columns has also been investigated with Eulerian-Lagrangian (continuous liquid phase and discrete gas phase) models (Zhang et al., 2013). The major works in this field have looked at different geometry bubble columns with drag force, virtual mass force, lift force primarily with two dimensional geometries (Buwa et al., 2006; Göz et al., 2004a,b; Luo and Al-Dahhan, 2011; Ekambara et al., 2005; Lain et al., 2002; Mouza et al., 2004). These studies looked at the sensitivity of the columns to such parameters and conditions as turbulence model, sparger location, superficial gas velocity, reactor aspect ratio and virtual mass.

#### *Limitations of Bubble Column Studies*

The main strength of these bubble column CFD models is that they are applied to general simple geometries, as the main focus was to isolate the bubble flows to explain the effects of the principal hydrodynamic operating conditions and parameters. These general approaches to CFD modelling of bubble columns present a strong platform from which to commence photobioreactor simulations, but they also lead to limitations in the context of purple phototrophic bacteria for wastewater treatment. Even if solids are present in the system being modelled, phases are modelled as liquid and gas. Modelling approaches for solid phases require refinement, in which the solids are modelled as discrete particles,

and the liquid and gas phases are modelled as continuous phases. In addition, these cases used simple geometries, which will probably not be appropriate for photobioreactor modelling and design, as the irradiated surface to volume ratio plays an important role in reactor performance (Soman and Shastri, 2015). Another note is that the generality of these cases means that biochemical reactions and photon-biomass interactions were not included in the studies.

#### 2.4.2 Photobioreactor CFD Models

Most photobioreactor CFD models account for flow behaviour, and mixing, as is the case for generic bubble columns. The studies also include irradiance (or illuminance for algae), photon-biomass interaction, and reactor or vessel configuration. Geometry plays an important part in biomass activity and subsequent reactor performance (Bitog et al., 2011). The coupling of computational fluid dynamics with biochemical reactions is yet to be explored in depth (Bitog et al., 2011). The main photobioreactor geometries for algae for treatment of wastewater in a laboratory context include flat plate, tubular, torus and cubic tank geometries (Perner-Nochta and Posten, 2007). In terms of flow characteristics, bubble column and airlift reactors have been the most extensively explored for photobioreactors (Perner-Nochta and Posten, 2007)

There are several models relating to the design configuration of photobioreactors, particularly for algae cultivation. Bari et al. (2015) conducted a study on the effects of sparger placement on flow patterns and heat transfer within a photobioreactor. It was found that minor changes in placement of spargers had significant impacts on the flow profile and heat transfer. There was no consideration of hydrodynamic effects on photon availability for biomass, but it was stated that the results had implications on these effects. It is important to note that the effect of inlet sparger configuration and gas flow characteristics could have an effect on the mortality of cells (Camacho et al., 2000; Bitog et al., 2014). Other reactor geometry simulations include studies on baffle placement and their effects on biomass activity (Yu et al., 2009; Bitog et al., 2014; Soman and Shastri, 2015; Wang et al., 2014a; Marshall and Sala, 2011; Su et al., 2010).

Although previously mentioned models state the importance of light or irradiance delivery to the biomass, little has been done in CFD to include both gas, liquid and biomass flow profiles, and the effects of irradiance intensity on cell growth. However there are light dependent growth rate expressions that exist that could be incorporated into a CFD model (Molina Grima et al., 1996; Acién Fernández et al., 1999). Perner-Nochta and Posten (2007) conducted studies of suspended algae in a tubular photobioreactor with a helical mixer. The light expression was derived as a function of light path (assumed as one dimensional) and the biomass concentration. This function was a modification of the Beer-Lambert law (equation 1)

$$\frac{d\phi(z)}{dz} = -X\epsilon_\lambda(z) \cdot \phi(z) \quad (1)$$



Where:

$\phi$  = irradiance intensity (*e.g.*  $Wm^{-2}$ , photon flux, lux)

$z$  = unidirectional irradiance path ( $m$ )

$\epsilon_\lambda$  = attenuation coefficient

$X$  = biomass concentration ( $gVSS \cdot m^{-3}$ )

The radial exchange of the liquid phase was correlated with the variations in light intensity on the algal cells. The results in the case of the tubular reactor were compared to those where no static mixer was present. There was no effort to account for light dependent growth expressions in this work.

#### ***Limitations of Photobioreactor CFD Models***

There are several limitations and gaps arising from the previously mentioned works. Firstly, most algae CFD models consider mixing and flow profiles as the major bottleneck to photobioreactor performance. This raises questions as to how the selection of wavelength, irradiance intensity, placement of light or radiation sources, and optical properties of reactor materials have an ultimate effect on cell growth and photobioreactor performance. There has also been no integrated assessment of spatial flow dynamics, biochemical expressions, and photon-biomass interactions in existing CFD models (Wang et al., 2014b).

#### **2.4.3 Bioreactor Design Optimisation Models**

This section assesses the use of CFD models for general bioreactors, including biokinetic expressions. Incorporation of biochemical equations into mixing and fluid flow profile models is important as these systems of equations will need to be solved simultaneously, along with irradiance expressions, such that the optimal operating conditions of the proposed photo-anaerobic membrane bioreactor can be determined. There has been limited work done overall on the use of CFD in biokinetic systems.

Secondly, a review of anaerobic digester models has been conducted to assess in particular the rheology and settling characteristics of the different phases being modelled.

#### **Models incorporating spatio-temporal variations with biokinetic expressions**

Wang et al. (2010) conducted research into developing a three phase hydrodynamic Euler-Euler model of an expanded granular sludge bed reactor with coupled with biological reaction kinetics. The reactor was a fermenter for hydrogen production with glucose as the reactant. The hydrodynamics model was set up according to their previous work (Wang et al., 2009). The governing equations were solved over three phases –  $H_2$  gas, wastewater as liquid, and the sludge granules as the solid phase. Wastewater was assumed to display the same characteristics as pure water, and all phases were assumed incompressible, which in the gas phase was possible due to the small bubble diameter. The reaction of glucose was incorporated into the model with experimentally determined reaction rates. The rate of hydrogen production was then solved for different hydraulic



retention time (HRT) and inlet chemical oxygen demand (COD) concentration conditions ( $HRT = \{4\text{ h}, 2\text{ h}, 1\text{ h}\}$ ,  $COD = \{2000\text{ mgL}^{-1}, 4000\text{ mgL}^{-1}, 6000\text{ mgL}^{-1}, 8000\text{ mgL}^{-1}\}$ ). There was no consideration of biomass growth in this model.

A second study by Elqotbi, et. al., 2013 considered a more extensive model of a continuously stirred tank reactor (CSTR) (Elqotbi et al., 2013). The reactor produced gluconic acid by *Aspergillus niger*. The bioreaction equation species were the concentrations of; biomass, glucose substrate, dissolved oxygen, and gluconic acid product. The cell growth term was modelled using Monod kinetics. This model was validated against experimental data. The key differences between this study and the previous one are that in addition to flow characteristics, substrate uptake and product formation, efforts were made to account for cell growth and varying viscosity effects, which in turn gave a better approximation and explanation of the process.

### Anaerobic Digester Models

The use of CFD to understand mixing, heat transfer, rheology and biokinetic reactions has been reviewed extensively in a recent paper in which nine studies were analysed (Lindmark et al., 2014). The bulk of these studies analysed mixing with impellers, varying mixing to draw conclusions on the effect of impeller speed and placement on bulk fluid velocities to ensure there were no dead zones. In this sense, these studies are very similar to the previously mentioned bubble column and algae CFD models. The main difference is that the solid phase is modelled as a shear-thinning fluid in an Eulerian frame (Bridgeman, 2012; Craig et al., 2013).

### *Limitations of General Bioreactor and Anaerobic Digester CFD Models*

The main limitations of both the bioreactor models and anaerobic digester models are the failure to incorporate biochemical reactions into the model. This is possibly due to the vastly different time scales of fluid behaviour and the biochemical processes. This limitation was also highlighted in the PhD thesis of David Gaden (Gaden, 2013).

The major limitation of the anaerobic digester models when drawing inspiration for the modelling of phototrophic bacteria is that irradiance doesn't play a role in the former case, and as such, an Euler-Euler model is appropriate. In the case of a photon-biomass interaction CFD model, the better approach is to have the biomass modelled as discrete solid particles interacting with an irradiance front.

## 2.5 Pathogen Removal

Wastewater treatment exists primarily to protect public health (Jacangelo and Trussell, 2002). The first processes for WWT were therefore designed to inactivate or remove human enteric bacteria, protozoa and viruses (Ibarluzea et al., 2007; Jacangelo and Trussell, 2002). Different treatment methods and discharge concentration limits exist for different end purposes of the treated wastewater, but there is a necessity to remove or inactivate



pathogens so that the subsequent waterways don't become vectors for fecal-oral disease transmission in humans (Carducci et al., 2008).

### Current Techniques Pathogen Removal in Wastewater

Excluding post treatment solutions for the removal of pathogens such as chlorination, ozonation and UV disinfection, the activated sludge process is a mainline process which aids in reducing the enteric particle concentration from the liquid wastewater stream (Godfree and Farrell, 2005). The major mechanism by which pathogens are removed from the liquid stream by the activated sludge process is adsorption of enteric bacteria, protozoa and viruses on sludge agglomerates, as well as predation by the sludge, competition, and inactivation due to temperature, pH and sludge enzyme production (Chaudhry et al., 2015; Godfree and Farrell, 2005). This process is effective in treating the liquid stream, but this leaves a high pathogen concentration in the solids stream.

### Membrane Bioreactors as a Technology for Pathogen Removal

Membrane bioreactors (MBR) have demonstrated more efficient enteric pathogen removal compared to conventional WWT processes (Ottoson et al., 2006). In addition to separating sludge from the liquid stream, microfiltration membrane bioreactors retain bacteria to roughly 6 log reduction units (Lesjean et al., 2011). As viruses are smaller than the nominal pore size of microfiltration membranes, it is difficult to separate them physically by exclusion (Marti et al., 2011). Nevertheless, biological mechanisms such as adsorption to biomass, biofilm formation resulting in smaller effective membrane pore sizes, predation by biomass, and inactivation by enzymes produced by the biomass allow for effective removal of viral pathogens (Chaudhry et al., 2015). Other techniques in combination with membranes, such as photocatalytic inactivation of pathogens with subsequent membrane filtration have been proposed as effective pathogen reduction configurations (Mozia et al., 2014). However the majority of studies on MBR for pathogen removal are on aerobic systems. The efficacy of anaerobic membrane bioreactors (AnMBR) in removing pathogens is yet to be explored in a domestic wastewater treatment context. A study by (Wong et al., 2009) demonstrated a 6 log CFU reduction for *E. coli* and *C. perfringens* and a 3.7 log PFU reduction of coliphages. The results of the bacterial and protozoan reductions were attributed to the presence of the membrane. The nominal pore size of the membrane was  $0.03 \mu\text{m}$ , which would account for the incomplete removal of coliphages from the anaerobic digester effluent. Other studies have reported high colophage removal efficiencies with larger membrane pore size (Lv et al., 2006; Ottoson et al., 2006; Ueda, 2000).

### Existing Modelling Techniques for Modelling Pathogens in Wastewater Treatment

The form of the pathogen (bacterium, protozoan or virus), influences modelling techniques, particularly for filtration (Ottoson et al., 2006). Bacteria and protozoa, often having diameters larger than the nominal pore size of the membrane, are retained in the solid phase of the reactor (Chaudhry et al., 2015). Viruses on the other hand are gener-



ally smaller than the membrane's pores, such that the mechanisms of their removal are different. These mechanisms are well understood for activated sludge processes, and these mechanisms can be extrapolated to AnMBRs as first order adsorption and inactivation processes (Haun et al., 2014; Chaudhry et al., 2015; Dias et al., 2015).

The methods for modelling these removal processes can be deterministic or stochastic in nature. The advantage of a stochastic approach is that one can account for natural random variations and propagate this uncertainty through processes (Hangos and Cameron, 2001; Batstone, 2013). A combination of both deterministic and stochastic components is usually applied without loss of generality and ability to explain the mechanisms of the process (Hangos and Cameron, 2001). The models developed for pathogen removal in wastewater have, for the most part, been constructed as lumped systems, with the assumption that the system is well mixed, so that the occlusion, adsorption, predation or inactivation of pathogens is only time dependent. Little work has been done on spatio-temporal models for pathogen removal in a wastewater treatment process, nor does there exist a purely stochastic model for which one can quickly develop, simulate and visualise without the need to collect large quantities of data.

## 2.6 Summary of Research Gaps

Based on the limitations foregrounded in the literature review, the following research gaps have been identified;

- The only existing application of PPB models are for hydrogen production or for explaining mechanisms their metabolism. No model has dealt with mixed cultures, and none have been applied to the treatment of wastewater.
- Pathogen removal models in wastewater treatment have been primarily concerned with running batch tests to fit parameters of first order differential equations. This process is expensive and cumbersome. The development of a model based on less arduous sampling processes is required.
- CFD has proven itself a promising method for understanding spatio-temporal variations of states in algae photobioreactors, however there exists only one model accounting for hydrodynamics, biokinetics and photon delivery, and no distributed parameter models in the case of PPB.
- As PPB for wastewater treatment is in its infancy as a technology, there currently exist no methods for optimising the plantwide the design of a PPB wastewater treatment process.

### 3 Research Objectives

Based on the summary of research gaps identified as a result of the critical literature review, the following objectives have been determined as novel and likely to make an impact within the scientific community.

#### 3.1 Research Objective 1

*Develop an adaptation of the IWA models to PPB for domestic wastewater treatment and simulate the model to visualise the most important processes and parameters.*

A mechanistic model will be developed based on standard IWA formate and nomenclature. The key parameters are; **1)** hydrolysis and fermentation, **2)** photoheterotrophic uptake of soluble organics,  $NH_4 - N$ , and  $PO_4 - P$ , **3)** chemoheterotrophic uptake, **4)** autotrophic uptake of inorganic carbon and hydrogen, and **5)** biomass decay.

#### 3.2 Research Objective 2

*Develop a generic stochastic model for pathogen removal in wastewater treatment processes.*

Most studies on pathogen removal technologies in wastewater treatment involve batch tests to identify the key parameters and differential equations of pathogen removal. Pathogen quantification methods are expensive, and models are developed using small datasets. It has been proposed that a stochastic pathogen removal model be built around small datasets with Markov chain Monte Carlo (MCMC) methods.

#### 3.3 Research Objective 3

*Quantify the interactions between cell growth and photon availability in order to extend the recently developed photoanaerobic model 1 (PAM1).*

Objective 3 aims to include irradiance into the model. The effects of photon incidence flux on biomass growth, maintenance, decay and inhibition will be determined and the resulting parameters will be used as input into CFD models.

#### 3.4 Research Objective 4

*Optimise the design of the PAnMBR for maximal performance and minimal operating costs (energy expenditure) and capital expenditure.*

This phase of research will draw on all previous objectives, along with concurrent studies within the CRC and larger research programme as a whole, in which valorisation methods of the PPB biomass will be explored. The PAnMBR design and operating conditions, as well as peripheral process units will be optimised in order to determine the best operating conditions for a range of industrial applications.

## 4 Methodology and Progress to Date

### 4.1 Research Objective 1

*Develop an adaptation of the IWA models to PPB for domestic wastewater treatment and simulate the model to visualise the most important processes and parameters.*

#### 4.1.1 Materials and Methods

Batch tests were carried out in 160 mL serum flasks with 100 mL of working volume made up of 10% v/v VSS as PPB, and 90% v/v Ormerod medium. Different operating conditions were run in order to isolate the different metabolic mechanisms identified. Parameters such as specific uptake rates, saturation constants, and inhibition constants were estimated based on the results of the batch tests. The model was then developed with the aid of a Petersen matrix, with mass balances over COD, N, P and inorganic carbon performed to calibrate the stoichiometric coefficients.

#### 4.1.2 Achievements to Date

The following information shows the rates equations for each mechanism and the resulting differential equations.

#### Hydrolysis

$$r_{hyd} = k_{hyd} \cdot X_c \quad (2)$$

#### Photoheterotrophy on acetate

$$r_{Ph,Ac} = k_{M,Ph,Ac} \cdot X_{PB} \cdot I_{FA} \cdot I_{IN} \cdot I_{IP} \cdot I_E \cdot \frac{S_{Ac}}{K_{S,Ac} + S_{Ac}} \quad (3)$$

#### Photoheterotrophy on other substrates

$$r_{Ph,SS} = k_{M,Ph,SS} \cdot X_{PB} \cdot I_{FA} \cdot I_{IN} \cdot I_{IP} \cdot I_E \cdot \frac{S_{SS}}{K_{S,SS} + S_{SS}} \quad (4)$$

#### Chemoheterotrophy

$$r_\chi = k_{M,\chi} \cdot X_{PB} \cdot I_{FA} \cdot I_{IN} \cdot I_{IP} \cdot \frac{S_{SS}}{K_{S,SS} + S_{SS}} \quad (5)$$

## Photoautotrophy

$$r_{At} = k_{M,ic} \cdot X_{PB} \cdot I_{FA} \cdot I_{IN} \cdot I_{IP} \cdot I_E \cdot \frac{S_{IC}}{K_{S,IC} + S_{IC}} \cdot \frac{S_{H2}}{K_{S,H2} + S_{H2}} \quad (6)$$

## Biomass Decay

$$r_{dec} = k_{dec} \cdot X_{PB} \quad (7)$$

## Inhibition Expressions

The expressions for inhibition are as follows;

### Inhibition due to free ammonia

$$I_{FA} = \frac{K_{I,FA}}{K_{I,FA} + S_{IN}} \quad (8)$$

### Inhibition due to inorganic nitrogen

$$I_{IN} = \frac{S_{IN}}{K_{S,IN} + S_{IN}} \quad (9)$$

### Inhibition due to inorganic phosphorus

$$I_{IP} = \frac{S_{IP}}{K_{S,IP} + S_{IP}} \quad (10)$$

### Inhibition due to irradiance

$$I_E = \frac{S_E}{K_{S,E} + S_E} \quad (11)$$

**Declaration of Parameter and Coefficient Values** The model was balanced over COD, C, N and P. The values for the stoichiometric coefficients and constants are contained in the draft paper presented in Appendix A.

In order to highlight and visualise the main mechanisms, the system of differential equations was implemented in Matlab. A Rosenbrock(2,3) ODE integrator method was used. The initial conditions loosely represented the domestic wastewater characteristics from Queensland Urban Utilities pump station SP118 in the 12 months from March 2014. The



Petersen matrix summarising the time-series evolution of state variables is available in Figure 4.

$j$	Component ( $C$ )	$\rightarrow$	$i$	1	2	3	4	5	6	7	8	9	10
	Process↓			$S_S$	$S_{Ac}$	$S_{IC}$	$S_{H2}$	$S_{IN}$	$S_{IP}$	$S_I$	$X_{PB}$	$X_C$	$X_I$
1	Hydrolysis/fermentation			$f_{ss,xc}$	$f_{SAC,xc}$	$f_{IC,xc}$	$f_{H2,xc}$	$f_{IN,xc}$	$f_{IP,xc}$	$f_{SI,xc}$	0	-1	$f_{xi,xc}$
2	Acetate uptake			0	-1	$f_{IC,ph,ac}$	0	$-f_{N,B}Y_{PB,ph}$	$-f_{P,B}Y_{PB,ph}$	0	$Y_{PB,ph}$	0	0
3	Photoheterotrophic uptake			-1	0	$-f_{IC,ph,ss}$	0	$-f_{N,B}Y_{PB,ph}$	$-f_{P,B}Y_{PB,ph}$	0	$Y_{PB,ph}$	0	0
4	Chemoheterotrophic uptake			-1	$(1 - Y_{PB,ch})$	0	$(1 - Y_{PB,ch})$	$-f_{N,B}Y_{PB,ch}$	$-f_{P,B}Y_{PB,ch}$	0	$Y_{PB,ch}$	0	0
5	Autotrophic uptake			0	0	$-f_{IC,a}$	$-f_{H2,a}$	$-f_{N,B}Y_{PB,a}$	$-f_{P,B}Y_{PB,a}$	0	$Y_{PB,a}$	0	0
6	Decay of XPB			0	0	$-\sum_{i=8}^9 C_i \times f_{C,i}$	0	$-\sum_{i=8}^9 C_i \times f_{N,i}$	$-\sum_{i=8}^9 C_i \times f_{P,i}$	0	-1	1	0
				Soluble substrate ( $\text{g COD L}^{-1}$ )	Acetate ( $\text{g COD L}^{-1}$ )	Inorganic carbon ( $\text{mg C}_\text{-HCO}_3 \text{L}^{-1}$ )	$H_2$ ( $\text{g COD L}^{-1}$ )	Inorganic nitrogen ( $\text{g N}_\text{-NH}_4 \text{L}^{-1}$ )	Inorganic phosphorous ( $\text{g P}_\text{-PO}_4 \text{L}^{-1}$ )				

Figure 4: Petersen matrix summarising rates of all metabolic mechanisms for PAM1

Three different cases were simulated. Firstly to demonstrate the dependence of the PPB reactor performance on particular initial concentrations of soluble COD and N, different initial values were varied and contour plots were constructed. Figure 5 demonstrates this dependence. The simulation was also carried out for the interdependencies of soluble COD and P. The darker sections of the plot indicate the concentrations at which uptake approaches 100% for both substrates.

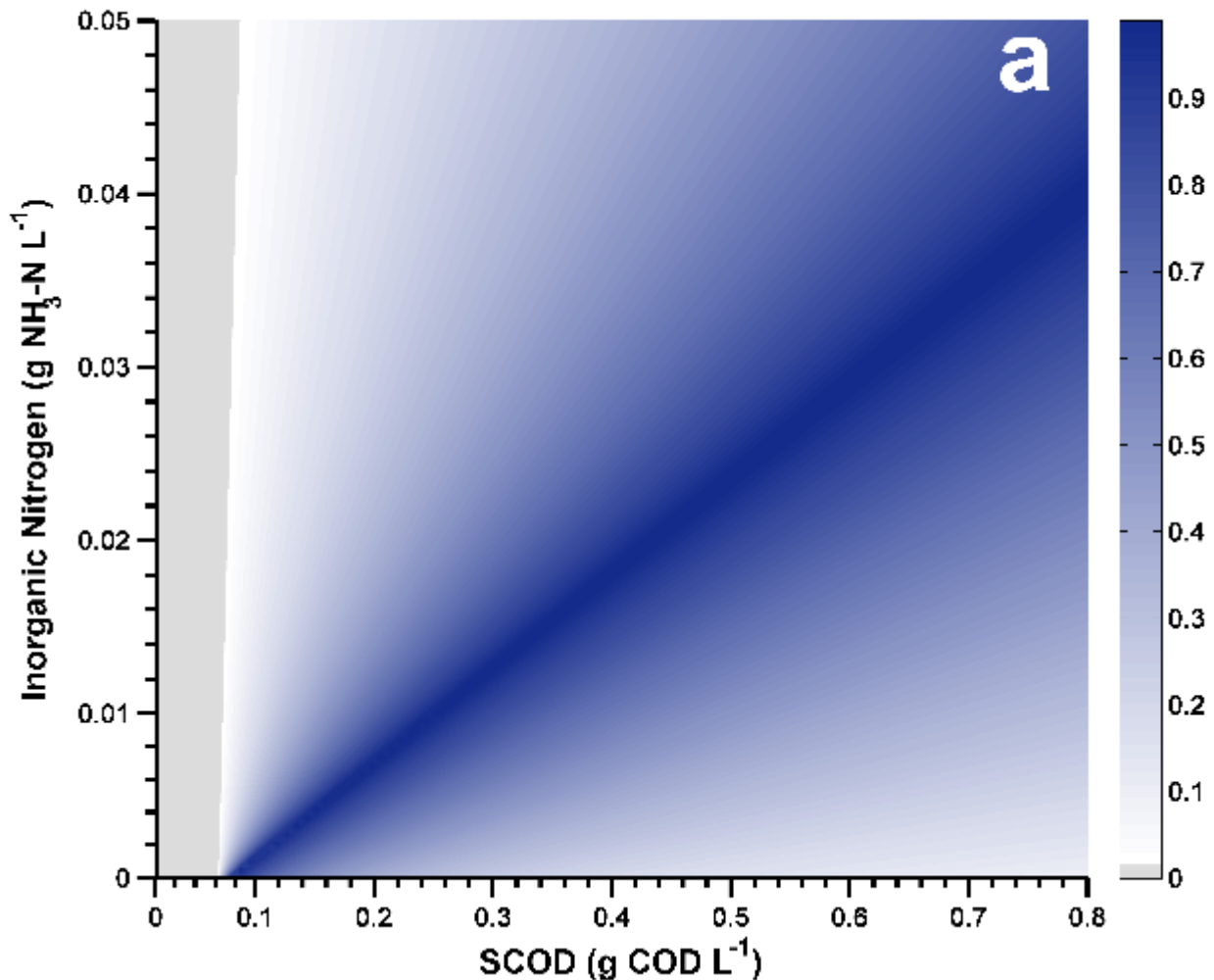


Figure 5: Dependence of the PAnMBR on initial concentrations of soluble COD and inorganic nitrogen

The third simulation (Figure 6) demonstrates the effects of irradiance cycling on the uptake of soluble COD substrates and biomass growth.

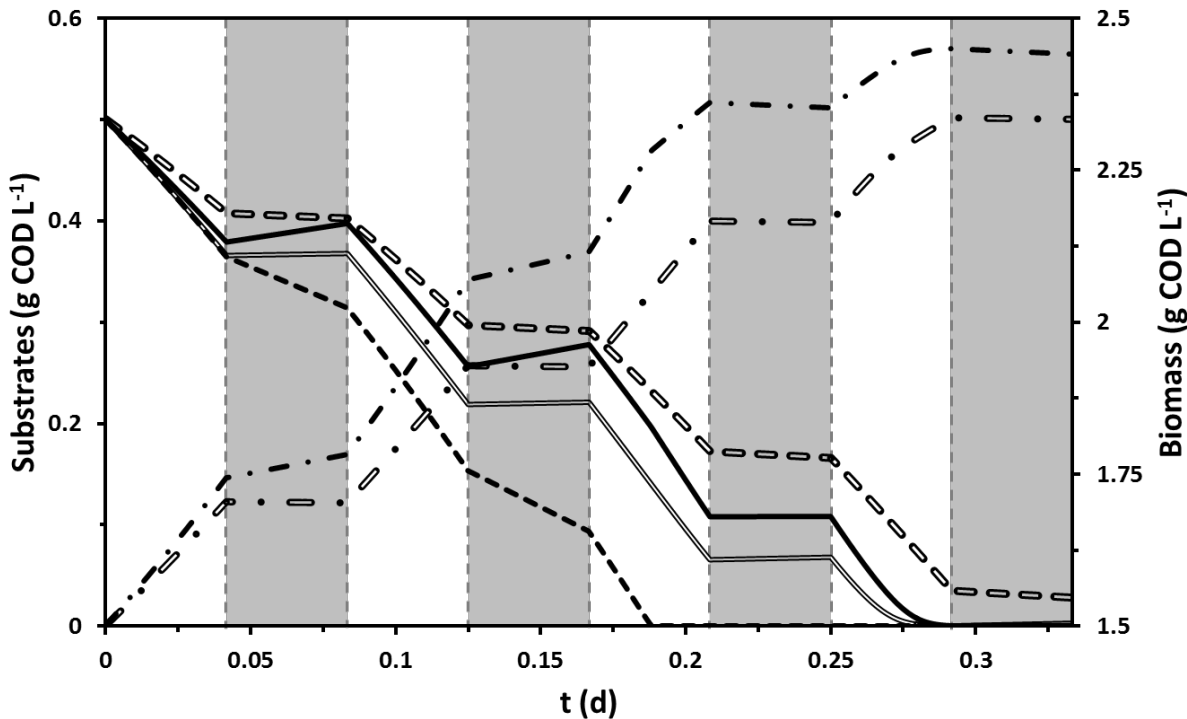


Figure 6: Effect of dark/light cycles on PPP metabolism under low (double lines) and high (single lines) chemoheterotrophic activity ( $k_{M, ch} = 0.074$  and  $0.7 \text{ g COD g}^{-1} \text{ COD d}^{-1}$ , respectively). Simulation of the evolution of acetate (continuous line), ethanol (dashed line), and biomass (dash-dot lines) concentrations during 1 h dark/light periods.

The final simulation served to highlight the difference in inorganic carbon photoautotrophic uptake rates  $k_{M, au}$  found in the literature and the one determined through batch experiments. The value determined through experiment was  $0.041 \text{ gC gCOD}^{-1} \text{ d}^{-1}$ . The uptake rates in literature were determined from hydrogen production applications. 10 000 random values of  $k_{M, au}$  were sampled from a generated normal distribution truncated to a 95% confidence interval with a mean and standard deviation of  $0.3 \text{ gC gCOD}^{-1} \text{ d}^{-1}$  and  $0.15 \text{ gC gCOD}^{-1} \text{ d}^{-1}$  respectively. Figure 7 demonstrates the effects of the uptake rate value on the concentration of inorganic carbon substrate.

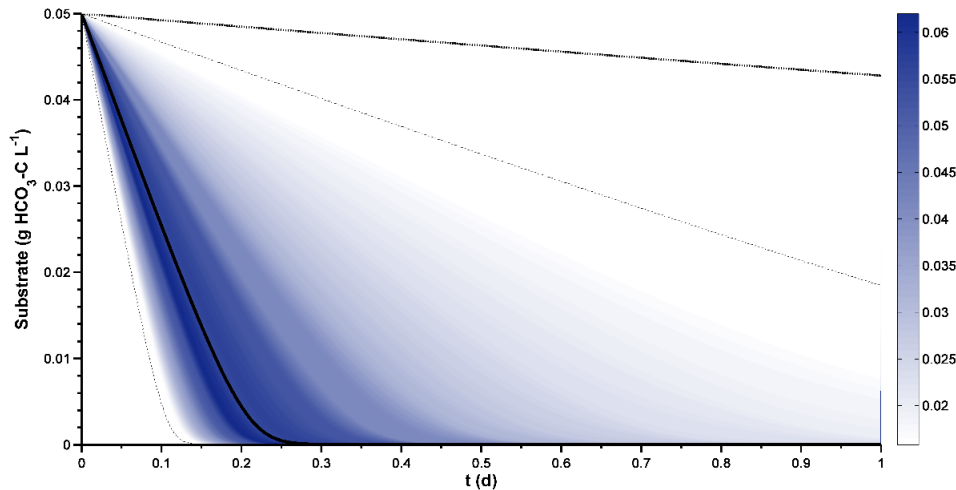


Figure 7: Photoautotrophic uptake of inorganic carbon. The blue region shows the literature values simulated 10 000 times. The darker colour denotes a higher probability of inorganic carbon uptake. The mean of the samples is plotted as a thick black line, and the 95% confidence limits are the two bounding dotted lines. The thick dotted line is the value determined in the batch tests with PPB from domestic wastewater.

#### 4.1.3 Conclusions

This model has been developed for the anaerobic treatment of domestic wastewater. It highlights the main metabolic mechanisms. Biological limitations include no nitrogen fixation, and no poly-P or carbon accumulation, but these are not dominant in the base system. The particular limitations which form the basis for Research Objective 3 are that hydrodynamics, and the integration of mechanistic photon-biomass interactions have not been included.

## 4.2 Research Objective 2

*Develop a generic stochastic model for pathogen removal in wastewater treatment processes.*

### 4.2.1 Materials and Methods

#### Experimental Methods

The performance of the lab-scale 2 L PAnMBR was demonstrated in a recently submitted paper (Hülsken et al., 2015). However, the efficacy of the system to remove key indicator pathogens had not been explored. As such, data were collected from the two PAnMBRs, one at an ambient temperature of  $22^{\circ}\text{C} \pm 2^{\circ}\text{C}$ , and the other at  $10^{\circ}\text{C} \pm 1^{\circ}\text{C}$ . Samples were taken from domestic wastewater sourced from Queensland Urban Utilities pump



station SP118 and maintained at 4 °C, with filtered (0.45  $\mu\text{m}$  Kubota flat plate membrane) and non-filtered domestic wastewater samples analysed.

The reactors were maintained with an hydraulic retention time (HRT) of 24 hours, and five sampling events will be extracted for two solids retention times each ( $SRT = \{2 \text{ d}, 4 \text{ d}\}$ ).

The pathogen quantification methods for *E. coli*, *C. perfringens*, and somatic coliphages are summarised in Table 3.

Table 3: Indicator pathogen quantification methods

Indicator Pathogen	Quantification Method
<i>E. coli</i>	Chromocult Coliform agar (Merck KGaA, Germany) with <i>E. coli</i> /coliform Selective Supplement (Merck KGaA, Germany) and plates incubated at 37 °C for 20 ± 4 h
<i>C. perfringens</i>	SPS (sulphite polymyxin sulphadiazine) agar (Cultimed, Scharlau) after a thermal shock at 80 °C for 10 min. All samples incubated at 44 °C for 20 ± 4 h under anaerobic conditions.
Somatic Coliphages (SOMCPH)	enumerated by the double-agar-layer method following the ISO standard 10705-2. Plaque forming units (PFUs) of SOMCPH are counted in the WG5 <i>E. coli</i> strain after 20 ± 4 h incubation at 37 °C.

## Modelling Methods

The three indicator pathogens will be assigned states based on the recollected data. These states include;

- detected D (the organism is alive and has not experienced the effects of the removal technique)
- non-detected  $\bar{D}$  (the organism is either inactivated, has been filtered by the membrane, or has adsorbed to sludge flocs)

The probability that the pathogen belongs to one of these binary states will be determined and a truncated t distribution with support in [0,1] will be generated for the possible states. A resulting transition matrix, which defines the probability of a pathogen in state  $i$  either remaining in the same state or moving to state  $j$  can then be constructed. A transition matrix ( $T_{ij}$ ) (2 × 2 in this binary case) can be constructed as follows;

$$\mathbb{P}(j|i) = T_{ij} \quad (12)$$

The transition matrix must satisfy the following condition, which stems from its definition;

$$\forall j, \quad \sum_j \mathcal{T}_{i,j} = 1 \quad (13)$$

The model will then action an appropriate number of indicator pathogens ( $10^{10}$  *E. coli*,  $10^5$  *C. perfringens*, and  $10^5$  SOMCPH) each with initial states of  $[D \bar{D}] = [1 \ 0]$ . The model will be run for  $n$  time steps. The probability that the organism be in either of the states at time step  $n$  will only depend on its state at time step  $n-1$ . This will be a generic algorithm which will be able to be applied to different pathogen removal techniques for domestic wastewater treatment.

#### 4.2.2 Achievements to Date

The sampling and detection of the indicator pathogens has been carried out. The results have been summarised in Table 4 for both mesophilic and psychrophilic reactors over the two different SRTs.

Table 4: Results for the sampling carried out between April 2015 and July 2015. The results have been expressed as average log reductions to a 95% confidence interval.

**SRT 2**

	<i>E. coli</i>	<i>C. perfringens</i>	SOMPCH
<b>Mesophilic</b>	$5.90 \pm 0.89$	$4.55 \pm 0.31$	$0.80 \pm 0.27$
<b>Psychrophilic</b>	$5.45 \pm 1.18$	$4.52 \pm 0.49$	$0.90 \pm 0.32$

**SRT 4**

	<i>E. coli</i>	<i>C. perfringens</i>	SOMPCH
<b>Mesophilic</b>	$6.01 \pm 0.68$	$4.52 \pm 0.68$	$0.54 \pm 0.67$
<b>Psychrophilic</b>	$5.60 \pm 1.22$	$4.46 \pm 0.50$	$0.49 \pm 0.56$

It was decided that due to the relatively poor log reductions through the PAnMBR system, the model would be developed as a more generalised approach. Inactivation data from peracetic acid dosing at a chemically enhanced primary treatment plant in San Diego, California has been sourced from Trojan Technologies, Ontario Canada and will be used to validate the generic model.

#### 4.2.3 Expected Outcomes

It is expected that the work will be drafted for publication prior to Nov 2015 and prior to my departure for Canada. This model will be of benefit to the quantitative microbial risk analysis (QMRA) community because fewer sampling events are required to develop an understanding of the uncertainty in performance of a pathogen removal system.



## 4.3 Research Objective 3

*Quantify the interactions between cell growth and photon availability in order to extend the recently developed photoanaerobic model 1 (PAM1).*

This objective forms the major part of the thesis. There are numerous steps to be taken in order to extend PAM1.

### 4.3.1 Materials and Methods

#### Selection of Wavelengths and Intensities

The recent acquisition of the Stellarnet BlueWave spectroradiometer will allow the rigorous determination of the particular wavelengths and irradiances and their effects on the growth, maintenance and decay of the PPB biomass. It has been well documented that the light harvesting complexes absorb several different wavelengths as per Figure 8, although energy consumption for artificial light sources will form a major part of operating expenses. This is why it is important to quantify the activity and growth of PPB with different combinations of wavelengths.

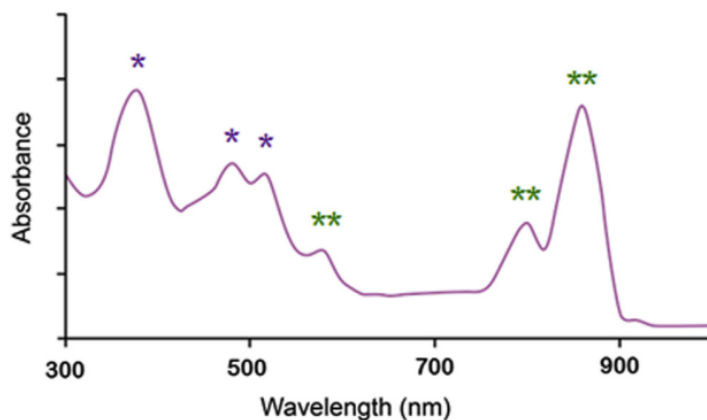


Figure 8: Absorbance spectrum of typical PPB. The purple stars show wavelengths at which carotenoids absorb photons, and the green stars show where bacteriochlorophylls absorb photons (Adessi and De Philippis, 2014)

Following this, the effects of different irradiance intensities on biomass activity and growth, as well as the effects of biomass, inert solids, water, soluble compounds and metals on the attenuation of light will be quantified.

#### Hydrodynamics Study of PAnMBR

As determined in the literature review, mixing and flow profiles play an important role in the delivery of photons to the system. It is therefore proposed that two and three dimensional simulations be carried out on a pilot scale ( $1 \text{ m}^3$ ) PAnMBR. These studies will be conducted in the OpenFOAM open source computational fluid dynamics toolbox.



Simulations will be carried out with variations on reactor geometry, gas flow rate, bubble size, membrane position, rheological properties of the bulk non-newtonian liquid, and temperature. An Euler-Euler reference frame will be the most appropriate for this phase of research. For these studies to be achieved seamlessly, it will be important to learn Python scripting for efficiently generating bulk geometry variations in Salomé 7.6.0, an open source computer aided design (CAD) and meshing software used by Électricité de France for CFD preprocessing.

### Incorporation of Hydrodynamics and Irradiance Models

This phase will see the hydrodynamics model revised to include three phases (gas, liquid wastewater, and solid PPB biomass). The solid PPB particles will be tracked to assess their exposure to the light source. Dead zones and problematic areas within the reactor will be identified and modifications to the geometry design and light source intensity will be made.

### Overlaying of PAM1

The PAM1 will be superimposed once the hydrodynamics and irradiance studies are complete in order to visualise the spatio-temporal variations in the uptake of substrates according to the processes determined in PAM1.

#### 4.3.2 Achievements to Date

Within the research group, work is being done to scale up the PAnMBR to a  $1\ m^3$  vessel. Designs for a vessel from Kellogg Brown Root (KBR) were provided, and a hydrodynamic study was attempted in OpenFOAM. Due to discontinuities in the design, and its overall complexity, modifications had to be made to ensure quality meshing and results.

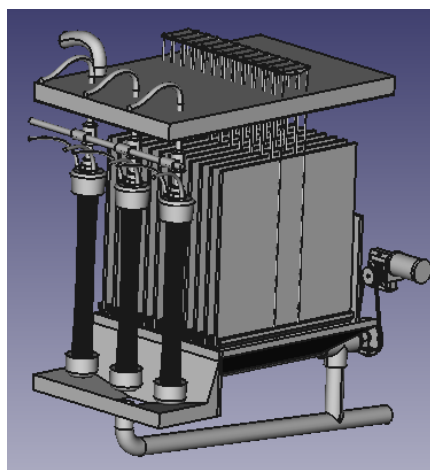


Figure 9: Initial design by KBR

The reactor was simplified to a 2D geometry, and was meshed in Salomé with tetrahedral

volumes. The geometry and meshing elements are 3 dimensional as OpenFOAM only allows 3 dimensional cases. The mesh was organised as a projection from one face to another, with a 1 element thickness for the dimension not being solved for. The dimensions of the reactor in Figure 10 are;

- Height  $\Delta y = 1.05$  m
- Length  $\Delta z = 0.97$  m

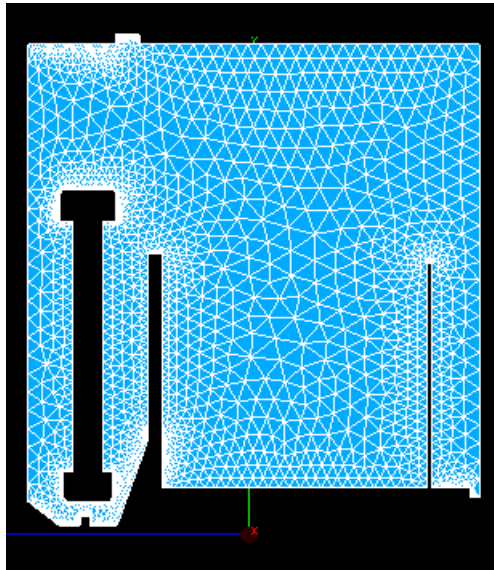


Figure 10: Two dimensional mesh generated in Salomé

The solver used in this study was OpenFOAM's **twoPhaseEulerFoam**. The vessel was modelled as a bubble column. Although won't be used as sparging gas in the real situation, air was used as the gas to be recycled through the reactor. The initial flow rate was 20 L/min. Further studies are required with different flow rates.

Figure 11 shows the solution after 10 seconds of operation. The sparger is located in the bottom left hand corner of the reactor, just below the membrane. An extra weir was placed behind the membrane in order to achieve better mixing. More studies on weir placement will be required to further optimise the fluid flow behaviour of the PAnMBR.

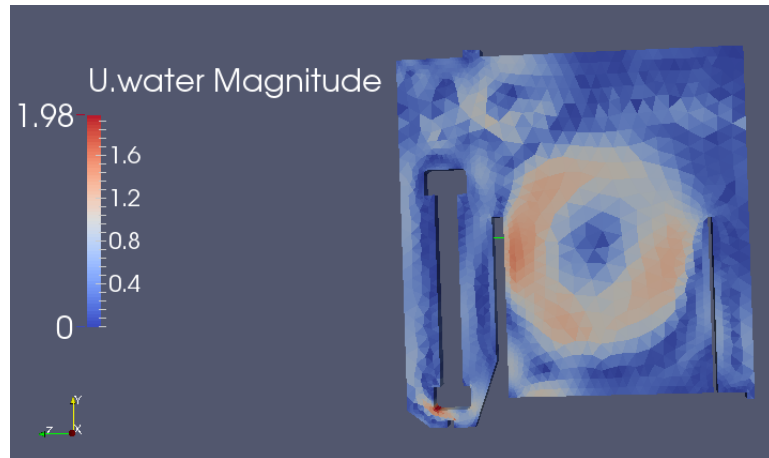


Figure 11: Eddy formation after 10 s of operation

#### 4.3.3 Expected Outcomes

The hydrodynamic study will need to be refined, and solved over a 3D vessel. In this study, the placement of weirs and flow rates of membrane sparging gas will be varied in order to find the best operating conditions of the PAnMBR. It is expected that I will travel to Trojan Technologies, Ontario, Canada in order to refine the hydrodynamics and irradiance models.

With the arrival of the spectroradiometer, batch tests will be conducted to determine the most efficient combinations of wavelengths and irradiances for cell growth and reactor performance. The results from these tests will be incorporated into the hydrodynamic study, in which the dependency of the light penetration on reactor geometry and non biological reactor contents will be modelled. A third lagrangian solid phase will be introduced to the model. Sensitivity analyses on the reactor geometry, operating irradiance, solids concentration, and mixing characteristics will be performed. It is expected that this work will lead to output of publication standard.

The results from this work will be combined with the findings from Research Objective 1, in which the mechanistic biokinetic expressions will overlay the previous work. Numerically, this will be a delicate process, as the time scales of the flow regimes, the irradiance, and the biochemical equations are vastly different. These problems were encountered when David Gaden attempted to combine ADM1 with 3 dimensional variations (Gaden, 2013). These problems were highlighted as limitations of the model, and it was identified that further work was required for improvement.

## 4.4 Research Objective 4

*Optimise the design of the PAnMBR for maximal performance and minimal operating costs (energy expenditure) and capital expenditure.*

### 4.4.1 Materials and Methods

This work is concerned with amassing the previous research objectives in order to optimise a full scale reactor design. As such, the previous research objectives must be completed before this phase can commence.

### 4.4.2 Expected Outcomes

The overall goal of Research Objective 4 is to extend the theory and outcomes from Research Objectives 1 and 3 in order to optimise the design of the PAnMBR. Different materials of construction will be considered, and a technological and economic feasibility analysis will be carried out based on these results.

## 4.5 Timeline

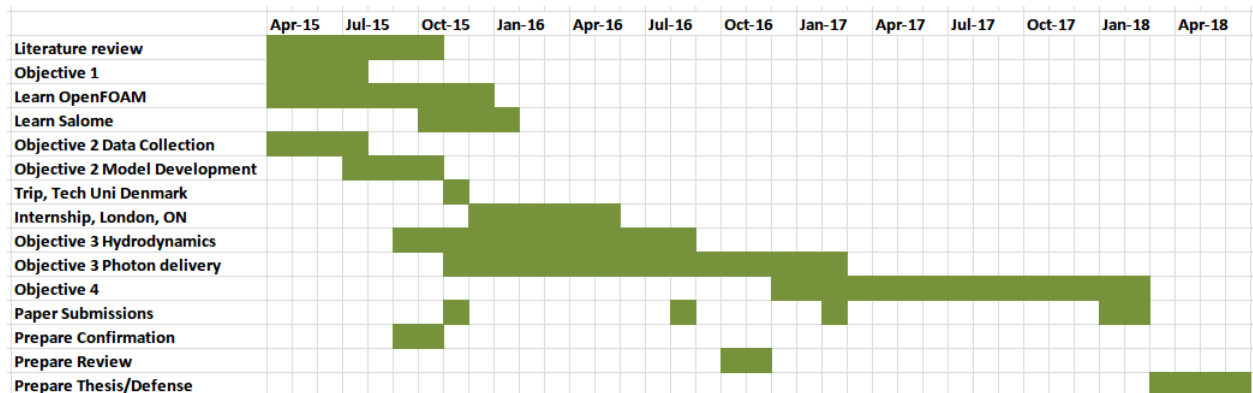


Figure 12: Timeline for PhD work

## References

- Acién Fernández, F. G., García Camacho, F., and Chisti, Y. (1999). Photobioreactors: light regime, mass transfer, and scaleup. *Progress in Industrial Microbiology*, 35(C):231–247.
- Adessi, A. and De Philippis, R. (2014). Photobioreactor design and illumination systems for H<sub>2</sub> production with anoxygenic photosynthetic bacteria: A review. *International Journal of Hydrogen Energy*, 39(7):3127–3141.
- Baghbanzadeh, S. and Kassal, I. (2015). Purple-bacterial light harvesting benefits more from energy funnelling than from delocalisation. *arXiv pre-print*. <http://arxiv.org/abs/1509.01537>, pages 1–11.
- Bari, G. S., Suess, T. N., Anderson, G. a., and Gent, S. P. (2015). Hydrodynamic and Heat Transfer Effects of Varying Sparger Spacing Within a Column Photobioreactor Using Computational Fluid Dynamics. *Journal of Fuel Cell Science and Technology*, 12(1):011004.
- Batstone, D., Hülsken, T., Mehta, C., and Keller, J. (2015). Platforms for energy and nutrient recovery from domestic wastewater: A review. *Chemosphere*, 140:2–11.
- Batstone, D. J. (2013). Teaching uncertainty propagation as a core component in process engineering statistics. *Education for Chemical Engineers*, 8(4):e132–e139.
- Batstone, D. J., Keller, J., and Steyer, J. P. (2006). A review of ADM1 extensions, applications, and analysis: 2002–2005. *Water Science and Technology*, 54(4):1–10.
- Bitog, J. P., Lee, I. B., Lee, C. G., Kim, K. S., Hwang, H. S., Hong, S. W., Seo, I. H., Kwon, K. S., and Mostafa, E. (2011). Application of computational fluid dynamics for modeling and designing photobioreactors for microalgae production: A review. *Computers and Electronics in Agriculture*, 76(2):131–147.
- Bitog, J. P. P., Lee, I. B., Oh, H. M., Hong, S. W., Seo, I. H., and Kwon, K. S. (2014). Optimised hydrodynamic parameters for the design of photobioreactors using computational fluid dynamics and experimental validation. *Biosystems Engineering*, 122:42–61.
- Bridgeman, J. (2012). Computational fluid dynamics modelling of sewage sludge mixing in an anaerobic digester. *Advances in Engineering Software*, 44(1):54–62.
- Buwa, V. V., Deo, D. S., and Ranade, V. V. (2006). Eulerian-Lagrangian simulations of unsteady gas-liquid flows in bubble columns. *International Journal of Multiphase Flow*, 32(7):864–885.
- Buwa, V. V. and Ranade, V. V. (2002). Dynamics of gas-liquid flow in a rectangular bubble column : experiments and single/multi-group CFD simulations. *Chemical Engineering Science*, 57:4715–4736.



- Camacho, F. G., Gómez, a. C., Sobczuk, T. M., and Grima, E. M. (2000). Effects of mechanical and hydrodynamic stress in agitated, sparged cultures of *Porphyridium cruentum*. *Process Biochemistry*, 35(9):1045–1050.
- Carducci, A., Morici, P., Pizzi, F., Battistini, R., Rovini, E., and Verani, M. (2008). Study of the viral removal efficiency in a urban wastewater treatment plant. *Water science and technology*, pages 893–897.
- Chaudhry, R. M., Nelson, K. L., and Drewes, J. E. (2015). Mechanisms of pathogenic virus removal in a full-scale membrane bioreactor. *Environmental science & technology*, 49(5):2815–22.
- Cogdell, R. J., Gall, A., and Köhler, J. (2006a). The architecture and function of the light-harvesting apparatus of purple bacteria: from single molecules to in vivo membranes. *Quarterly reviews of biophysics*, 39(3):227–324.
- Cogdell, R. J., Gall, A., and Köhler, J. (2006b). The architecture and function of the light-harvesting apparatus of purple bacteria: from single molecules to in vivo membranes. *Quarterly reviews of biophysics*, 39(3):227–324.
- Cordell, D., Drangert, J. O., and White, S. (2009). The story of phosphorus: Global food security and food for thought. *Global Environmental Change*, 19(2):292–305.
- Craig, K., Nieuwoudt, M., and Niemand, L. (2013). CFD simulation of anaerobic digester with variable sewage sludge rheology. *Water Research*, 47(13):4485–4497.
- Dias, E., Dias, E., Ebdon, J., and Taylor, H. (2015). The application of removal coefficients for viruses in different wastewater treatment processes calculated using stochastic modelling. *Water science and technology*, 71(9):1382–1388.
- Ekambara, K., Dhotre, M. T., and Joshi, J. B. (2005). CFD simulations of bubble column reactors: 1D, 2D and 3D approach. *Chemical Engineering Science*, 60(23):6733–6746.
- Elqotbi, M., Vlaev, S. D., Montastruc, L., and Nikov, I. (2013). CFD modelling of two-phase stirred bioreaction systems by segregated solution of the Euler-Euler model. *Computers and Chemical Engineering*, 48:113–120.
- Gaden, D. (2013). *Modelling anaerobic Digesters in Three Dimensions: Integration of Biochemistry with Computational Fluid Dynamics*. PhD thesis.
- Godfree, A. and Farrell, J. (2005). Processes for Managing Pathogens. *Journal of Environmental Quality*, 34(1):105–113.
- Golomysova, A., Gomelsky, M., and Ivanov, P. S. (2010). Flux balance analysis of photo-heterotrophic growth of purple nonsulfur bacteria relevant to biohydrogen production. *International Journal of Hydrogen Energy*, 35(23):12751–12760.



- Gordon, G. C. and McKinlay, J. B. (2014). Calvin cycle mutants of photoheterotrophic purple nonsulfur bacteria fail to grow due to an electron imbalance rather than toxic metabolite accumulation. *Journal of Bacteriology*, 196(6):1231–1237.
- Göz, M., Laín, S., and Sommerfeld, M. (2004a). Study of the numerical instabilities in Lagrangian tracking of bubbles and particles in two-phase flow. *Computers & Chemical Engineering*, 28(12):2727–2733.
- Göz, M., Laín, S., and Sommerfeld, M. (2004b). Study of the numerical instabilities in Lagrangian tracking of bubbles and particles in two-phase flow. *Computers & Chemical Engineering*, 28(12):2727–2733.
- Hangos, K. M. and Cameron, I. T. (2001). *Process modelling and model analysis*. Academic Press, 4 edition.
- Haun, E., Haun, E., Ulbricht, K., Nogueira, R., and Rosenwinkel, K. H. (2014). Virus elimination in activated sludge systems: from batch tests to mathematical modeling. *Water science and technology*, 70(6):1115–1121.
- Hellingwerf, K. J., Crielaard, W., Hoff, W. D., Matthijs, H. C., Mur, L. R., and van Rotterdam, B. J. (1994). Photobiology of bacteria. *Antonie van Leeuwenhoek*, 65(4):331–347.
- Hülsen, T. (2015). *Nutrient recovery from domestic wastewater with purple phototrophic bacteria (in submission)*. PhD thesis.
- Hülsen, T., Barry, E. M., Lu, Y., Puyol, D., and Batstone, D. J. (2015). Low temperature treatment of domestic wastewater by purple phototrophic bacteria: performance, activity, and community. *Water Research (in submission)*.
- Hülsen, T., Batstone, D. J., and Keller, J. (2014). Phototrophic bacteria for nutrient recovery from domestic wastewater. *Water Research*, 50:18–26.
- Hunter, C. N., Daldal, F., Thurnauer, M. C., and Beatty, J. T. (2008). *The Purple Phototrophic Bacteria*, volume 28. Springer.
- Ibarluzea, J. M., Moreno, B., Serrano, E., Larburu, K., Maiztegi, M. J., Yarzabal, A., and Santa Marina, L. (2007). Somatic coliphages and bacterial indicators of bathing water quality in the beaches of Gipuzkoa, Spain. *Journal of Water and Health*, 5(3):417–426.
- Jacangelo, J. G. and Trussell, R. R. (2002). International report: Water and wastewater disinfection - Trends, issues and practices. In *Water Science and Technology: Water Supply*, volume 2, pages 147–157.
- Klamt, S., Grammel, H., Straube, R., Ghosh, R., and Gilles, E. D. (2008). Modeling the electron transport chain of purple non-sulfur bacteria. *Molecular systems biology*, 4(156):156.



- Klamt, S., Schuster, S., and Gilles, E. D. (2002). Calculability analysis in underdetermined metabolic networks illustrated by a model of the central metabolism in purple nonsulfur bacteria. *Biotechnology and Bioengineering*, 77(7):734–751.
- Lain, S., Bröder, D., Sommerfeld, M., and Göz, M. (2002). Modelling hydrodynamics and turbulence in a bubble column using the Euler-Lagrange procedure. *International Journal of Multiphase Flow*, 28(8):1381–1407.
- Lapin, A. and Luebbert, A. (1994). Numerical simulation of the dynamics of two-phase gas-liquid flows in bubble columns. *Chemical Engineering Science*, 49(21):3661–3674.
- Lehr, F., Millies, M., and Mewes, D. (2002). Bubble-size distributions and flow fields in bubble columns. *AICHE Journal*, 48(11):2426–2443.
- Lesjean, B., Tazi-Pain, A., Thaure, D., Moeslang, H., and Buisson, H. (2011). Ten persistent myths and the realities of membrane bioreactor technology for municipal applications. *Water Science and Technology*, 63(1):32–39.
- Lindmark, J., Thorin, E., Bel Fdhila, R., and Dahlquist, E. (2014). Effects of mixing on the result of anaerobic digestion: Review. *Renewable and Sustainable Energy Reviews*, 40:1030–1047.
- Luo, H. P. and Al-Dahhan, M. H. (2011). Verification and validation of CFD simulations for local flow dynamics in a draft tube airlift bioreactor. *Chemical Engineering Science*, 66(5):907–923.
- Lv, W., Zheng, X., Yang, M., Zhang, Y., Liu, Y., and Liu, J. (2006). Virus removal performance and mechanism of a submerged membrane bioreactor. *Process Biochemistry*, 41(2):299–304.
- Marshall, J. S. and Sala, K. (2011). A stochastic Lagrangian approach for simulating the effect of turbulent mixing on algae growth rate in a photobioreactor. *Chemical Engineering Science*, 66(3):384–392.
- Marti, E., Monclús, H., Jofre, J., Rodriguez-Roda, I., Comas, J., and Balcázar, J. L. (2011). Removal of microbial indicators from municipal wastewater by a membrane bioreactor (MBR). *Bioresource Technology*, 102(8):5004–5009.
- Matassa, S., Batstone, D. J., Huelsen, T., Schnoor, J. L., and Verstraete, W. (2015). Can direct conversion of used nitrogen to new feed and protein help feed the world? *Environmental Science & Technology*, page 150327153639000.
- McCarty, P. L., Kim, J., and Bae, J. (2011). Domestic Wastewater Treatment as a Net Energy Producer – Can This be Achieved ? *Environmental Science and Technology*, 45:7100–7106.



Minkevich, I. G., Laurinavichene, T. V., and Tsygankov, a. a. (2004). Theoretical and experimental quantum efficiencies of the growth of anoxygenic phototrophic bacteria. *Process Biochemistry*, 39(8):939–949.

Molina Grima, E., Fernández Sevilla, J. M., Sánchez Pérez, J. a., and García Camacho, F. (1996). A study on simultaneous photolimitation and photoinhibition in dense microalgal cultures taking into account incident and averaged irradiances. *Journal of Biotechnology*, 45(1):59–69.

Mouza, K. a., Kazakis, N. a., and Paras, S. V. (2004). Bubble column reactor design using a CFD code. In *1st International Conference From Scientific Computing to Computational Engineering Athens*, pages 1–8.

Mozia, S., Darowna, D., SzymaÅski, K., Grondzewska, S., Borchert, K., Wróbel, R., and Morawski, A. W. (2014). Performance of two photocatalytic membrane reactors for treatment of primary and secondary effluents. *Catalysis Today*, 236:135–145.

Ottoson, J., Hansen, a., Björlenius, B., Norder, H., and Stenström, T. a. (2006). Removal of viruses, parasitic protozoa and microbial indicators in conventional and membrane processes in a wastewater pilot plant. *Water Research*, 40(7):1449–1457.

Pareek, V., Cox, S., Brungs, M., Young, B., and a.a. Adesina (2003). Computational fluid dynamic (CFD) simulation of a pilot-scale annular bubble column photocatalytic reactor. *Chemical Engineering Science*, 58(3-6):859–865.

Perner-Nochta, I. and Posten, C. (2007). Simulations of light intensity variation in photobioreactors. *Journal of Biotechnology*, 131(3):276–285.

Pfleger, D. and Becker, S. (2001). Modelling and simulation of the dynamic flow behaviour in a bubble column. *Chemical Engineering Science*, 56:1737–1747.

Sokolichin, A. and Eigenberger, G. (1999). Applicability of the standard k-epsilon turbulence model to the dynamic simulation of bubble columns: Part I. Detailed numerical simulations. *Chemical Engineering Science*, 54(13-14):2273–2284.

Soman, A. and Shastri, Y. (2015). Optimization of novel photobioreactor design using computational fluid dynamics. *Applied Energy*, 140:246–255.

Steffen, W., Richardson, K., Rockström, J., Cornell, S., Fetzer, I., Bennett, E., Biggs, R., Carpenter, S. R., de Wit, C. a., Folke, C., Mace, G., Persson, L. M., Veerabhadran, R., Reyers, B., and Sörlin, S. (2015). Planetary Boundaries: Guiding human development on a changing planet. *Science*, 347(6223):736.

Su, Z., Kang, R., Shi, S., Cong, W., and Cai, Z. (2010). Study on the destabilization mixing in the flat plate photobioreactor by means of CFD. *Biomass and Bioenergy*, 34(12):1879–1884.



- Szilvester, S., Raduly, B., Abraham, B., Lanyi, S., and Niculae, D. R. (2010). Mathematical Models for Domestic Biological Wastewater Treatment Process. *Environmental Engineering and Management Journal*, 9(5):629–636.
- Takacs, I., Patry, G., and Nolasco, D. (1991). A dynamic model of the clarification-thickening process. *Water Research*, 25(10):1263–1271.
- Tchobanoglous, G., Burton, F. L., Stensel, H. D., and Eddy, M. . (2003). *Wastewater Engineering: Treatment and Reuse*. McGraw-Hill higher education. McGraw-Hill Education.
- Ueda, T. (2000). Fate of indigenous bacteriophage in a membrane bioreactor. *Water Research*, 34(7):2151–2159.
- Versteeg, H. K. and Malalasekera, W. (2007). *An Introduction to Computational Fluid Dynamics: The Finite Volume Method*. Pearson Education Limited, Upper Saddle River, 2 edition.
- Verstraete, W., Van de Caveye, P., and Diamantis, V. (2009). Maximum use of resources present in domestic "used water". *Bioresource Technology*, 100(23):5537–5545.
- Wang, L.-l., Tao, Y., and Mao, X.-z. (2014a). A novel flat plate algal bioreactor with horizontal baffles: Structural optimization and cultivation performance. *Bioresource Technology*, 164:20–27.
- Wang, S.-K., Stiles, A. R., Guo, C., and Liu, C.-Z. (2014b). Microalgae cultivation in photobioreactors: An overview of light characteristics. *Engineering in Life Sciences*, 14(6):550–559.
- Wang, X., Ding, J., Guo, W. Q., and Ren, N. Q. (2010). A hydrodynamics-reaction kinetics coupled model for evaluating bioreactors derived from CFD simulation. *Bioresource Technology*, 101(24):9749–9757.
- Wang, X., Ding, J., Ren, N.-Q., Liu, B.-F., and Guo, W.-Q. (2009). CFD simulation of an expanded granular sludge bed (EGSB) reactor for biohydrogen production. *International Journal of Hydrogen Energy*, 34(24):9686–9695.
- Wong, K., Xagoraraki, I., Wallace, J., Bickert, W., Srinivasan, S., and Rose, J. B. (2009). Removal of viruses and indicators by anaerobic membrane bioreactor treating animal waste. *Journal of environmental quality*, 38(4):1694–1699.
- Wood, M. G., Greenfield, P. F., Howes, T., Johns, M. R., and Keller, J. (1995). Computational Fluid Dynamic Modelling of Wastewater Ponds to Improve Design. *Water Science and Technology*, 31(12):111–118.
- Yu, G., Li, Y., Shen, G., Wang, W., Lin, C., Wu, H., and Chen, Z. (2009). A novel method using CFD to optimize the inner structure parameters of flat photobioreactors. *Journal of Applied Phycology*, 21(6):719–727.

Zhang, Q., Wu, X., Xue, S., Liang, K., and Cong, W. (2013). Study of hydrodynamic characteristics in tubular photobioreactors. *Bioprocess and Biosystems Engineering*, 36(2):143–150.

1      **Appendix A**

2      **The phototrophic anaerobic model no 1 (PAM-1): a mechanistic  
3                   model for anaerobic phototrophs in wastewater applications**

4                   *D. PUYOL, E. BARRY, T. HUELSEN, KENN LU, J. KELLER, D. BATSTONE.*

5    JOURNAL SELECTED: WATER RESEARCH

6    NUMBERING (without tables and figures): 7999 words

7    NUMBER OF TABLES: 3

8    NUMBER OF FIGURES: 6

9    **ABSTRACT**

10    **TO BE COMPLETED AFTER PAPER CORRECTION.**

11    *Key words:* *Phototrophic bacteria, resource recovery, mechanistic modelling, Partition-Release-Recovery*

13    **INTRODUCTION**

14    As wastewater treatment shifts focus from just treatment, to also capture and recovery of organics  
15    and nutrients, novel concepts are emerging for treatment. A key approach is to utilise fast growing  
16    organisms to concentrate energy, nutrients, and trace compounds into the solid phase, and hence  
17    substantially reduce reactive removal of nitrogen and organics while enabling phosphorous  
18    recovery. This includes high-rate activated sludge, which can achieve 40% nitrogen removal in the  
19    primary stage through adsorption and assimilation (Jetten et al. 1997). Algae can also be used to  
20    partition, though the inability of mixed cultures to grow simultaneously in heterotrophic and  
21    photosynthetic mode is a challenge. Purple phototrophic bacteria are a promising new partitioning  
22    approach, which have been shown to completely remove nitrogen to discharge limits when  
23    sufficient organic carbon is present without the need for pure cultures, and using IR light only as a  
24    driver for growth (Hülsen et al. 2014).

25    PPB grow phototrophically rather than photosynthetically, and do not use water as an electron  
26    donor to produce oxygen and organics. They are among the most metabolically versatile organisms

27 on earth (Hunter et al. 2008). These bacteria can growth heterotrophically using a wide range of  
28 organic compounds, both in presence and absence of light (photoheterotrophy and  
29 chemoheterotrophy) (Hunter et al. 2008). But they can growth autotrophically as well by using  
30 infrared light as the energy driver for CO<sub>2</sub> fixation, and different inorganic electron donors for the  
31 lithotrophic process, as H<sub>2</sub>, Fe<sup>2+</sup>, S<sup>2-</sup> or S<sub>2</sub>O<sub>3</sub><sup>2-</sup> (cyclic anoxygenic photosynthesis) (Overmann and  
32 Garcia-Pichel 1998). Though they can grow in the presence of oxygen, they are extremely effective in  
33 anaerobic photoheterotrophic conditions (Gordon and McKinlay 2014, McKinlay and Harwood  
34 2010a). Their ability to recycle electrons during the cyclic anoxygenic photosynthesis gives them a  
35 very high efficiency on electrons cycles. They can even accumulate electrons in form of reduced  
36 cofactors that they need to dispose for redox balancing. This can be done through two main  
37 strategies: (i) ATP-driven hydrogen production by ferredoxin oxidation in the  
38 hydrogenase/nitrogenase system at the end of the electron transport chain (ETC), and (ii) increasing  
39 the assimilative growth by re-fixation of CO<sub>2</sub> via Calvin Cycle produced during heterotrophic  
40 metabolism (McKinlay and Harwood 2010a). These metabolic features give them the possibility of  
41 growing and over-competing other microorganisms in heterogeneous phototrophic environments  
42 that promote the microbial growth, as low-mid strength wastewater systems with low hydraulic  
43 retention times (HRT) (Hulsen et al. 2014).

44 PPB present also other interesting features for their use in wastewater systems. They are able to  
45 accumulate polymers as poly-phosphate (poly-P) (Liang et al. 2010), polysaccharides (Klein et al.  
46 1991), poly-β hidroxybutyrate (PHB) (Melnicki et al. 2009) and other poly-3(hydroxyalkanoates)  
47 (PHA) (Brandl et al. 1991). And, under an excess of organics and available energy, they can be the  
48 main actor in biogenic hydrogen systems (Basak and Das 2007).

49 PPB have been assessed for wastewater treatment, particularly for processing swine wastewater  
50 (Kim et al. 2004), latex rubber-sheet wastewater (Kantachote et al. 2005), tofu wastewater (Zhu et  
51 al. 1999), or sugar refinery wastewater (Yetis et al. 2000). However, most of these studies were  
52 focused more on hydrogen production rather than organics removal or nutrient recovery (Fang et al.  
53 2005, Lee et al. 2010, Tao et al. 2008). They have also been applied on domestic wastewater  
54 (DWW) in batch and continuous operation to completely remove nitrogen to discharge limits when  
55 sufficient organic carbon is present without the need for pure cultures, and using IR light only as a  
56 driver for growth (Hülsen et al. 2014). This enables complete treatment of wastewater in a single  
57 step at comparable hydraulic retention times and to a similar standard as activated sludge  
58 processes, without destruction of the nitrogen and phosphorous.

59 Modelling is ubiquitously used to design, benchmark, and analyse wastewater treatment systems,  
60 with the IWA Activate Sludge Model (ASM)-family models being probably the most well-known  
61 (Henze et al. 2006). The IWA anaerobic digestion model no. 1 (ADM-1) is the analogous model for  
62 domestic and industrial anaerobic systems (Batstone et al. 2002). The IWA Models, and wastewater  
63 modelling in general has generally applied first order hydrolysis for solids transformation (including  
64 decay), Monod for uptake kinetics and inverse Monod (non-competitive) for inhibition functions, and  
65 the use of COD for organics and molar for inorganic compounds. Obviously development of new  
66 technologies using novel vectors such as PPB requires development of a similar mechanistic model.

67 There are complex metabolic models based on PPB metabolism focused on comprehensive analyses  
68 of the electron transport chain (Golomysova et al. 2010, Klamt et al. 2002). Due to its complexity,  
69 this is motivated more on pure scientific development rather than a real field application. There has  
70 also been work done on modelling PPB to describe hydrogen production only (Eroglu 2008,  
71 Gadhamshetty et al. 2008, Obeid et al. 2009). However, these are limited to hydrogen production  
72 that is performed under full illuminative anaerobic conditions with organics in excess and lacking of  
73 ammonium. But due to DWW composition, the key controlling mechanisms of PPB in DWW fed  
74 situation are photoheterotrophy (mainly) as well as chemoheterotropy and photoautotrophy  
75 growth modes, depending on wastewater composition. Biochemical mechanisms as solids hydrolysis  
76 and biomass decay have to be addressed as well. Therefore, this work is aiming to propose a  
77 mechanistic model based on the utilization of PPB as partition agent in DWW treatment. The model  
78 is open for future upgrades to be applied to other conditions, as e.g. industrial wastewater  
79 treatment and/or other metabolic processes of interest.

## 80 MATERIALS AND METHODS

### 81 Inoculum source

82 Biomass was extracted from a lab-scale continuous phototrophic anaerobic membrane bioreactor  
83 (PAnMBR) treating DWW under stably operation for more than 300 d. Main details of the reactor  
84 operation are described elsewhere (Hulsen et al. 2015 REF-Continuous paper-).

### 85 Wastewater source

86 DWW was collected from Taringa wastewater lift station (Brisbane, Australia) and stored  
87 immediately in a cold room at 4 °C. The wastewater was allowed to settle in 200 L drums and  
88 afterwards used as primary settled wastewater. The wastewater contained on average: 572 (141)  
89 mg L<sup>-1</sup> total chemical oxygen demand (TCOD); 241 (45) mg L<sup>-1</sup> soluble COD (SCOD); 45 (6) mg L<sup>-1</sup> NH<sub>4</sub><sup>-</sup>  
90 N; 63 (8) mg L<sup>-1</sup> total Kjehdahl Nitrogen (TKN), 5.6 (0.7) mg L<sup>-1</sup> PO<sub>4</sub>-P and 9 (1) mg L<sup>-1</sup> total

91 phosphorus (TP). The pH was 7.7 (0.3). Values in parentheses represent standard deviations across  
92 15 time series samples.

### 93 **Synthetic medium**

94 Synthetic Ormerod medium was used to explore single metabolic mechanisms. The medium  
95 contained (in mg L<sup>-1</sup>): MgSO<sub>4</sub>·7H<sub>2</sub>O (200), CaCl<sub>2</sub>·2H<sub>2</sub>O (75), FeSO<sub>4</sub>·7H<sub>2</sub>O (11.8), EDTA (20), yeast  
96 extract (30) and 1 mL L<sup>-1</sup> of a trace elements solution for a total concentration of: H<sub>3</sub>BO<sub>3</sub> (2.8),  
97 MnSO<sub>4</sub>·H<sub>2</sub>O (1.73), NaMoO<sub>4</sub>·2H<sub>2</sub>O (0.75), ZnSO<sub>4</sub>·7H<sub>2</sub>O (0.24), CuCl<sub>2</sub>·2H<sub>2</sub>O (0.135) and Riboflavin  
98 (0.2). Nitrogen was provided as NH<sub>4</sub>Cl, whereas phosphorus was added as KH<sub>2</sub>PO<sub>4</sub>. pH was fixed at  
99 7.5 by using a 1M NaOH solution. Media was buffered by using several buffer systems, and different  
100 organic and inorganic substrates were explored as specified below.

### 101 **Batch experiments**

#### 102 **Analysis of metabolism of PPB**

103 Anaerobic batch tests were conducted in 160 mL serum bottles inoculated with fresh biomass from  
104 the PAnMBR reactor. Working volume was fixed at 100 mL. The headspace was flushed with N<sub>2</sub>  
105 before adding the substrate. The experiments were carried out at room temperature (25-32 °C) in an  
106 orbital shaker set at 150 rpm (Edwards Instrument Company). Light experiments were illuminated  
107 with 2 x 150 W fluorescence lamps (Nelson Clamp Flood Light) from both sites. The bottles were  
108 covered with a UV-VIS absorbing foil (ND 1.2 299, Transformation Tubes). More details are described  
109 elsewhere (Hulsen et al. 2014). Different set-ups were carried out depending on the metabolic  
110 mechanisms analysed, as described in Table 1. All the experiments were accompanied by blank tests,  
111 where no substrate was supplemented, and, where needed, by positive and negative controls.

112 **Table 1:** Batch conditions of the different metabolic tests.

Mechanism	Medium	Buffer system*	COD/N/P (C/N/P)***	C source (mg COD L <sup>-1</sup> )	Energy source	Electron donor (mg L <sup>-1</sup> )	Electron acceptor	Positive control	Negative control
Photoheterotrophy	Ormerod	HEPES	100/10/2	Acetate (130), propionate, butyrate, ethanol (100)	Light	Organic	CO <sub>2</sub>	Adding 1 g NaHCO <sub>3</sub>	-
Nitrogen limitation	Ormerod	HEPES	100/1.4/2	Acetate (130)	Light	Organic	CO <sub>2</sub>	No N limitation	-
Phosphorus limitation	Ormerod	HEPES	100/10/0.15	Acetate (130)	Light	Organic	CO <sub>2</sub>	No P limitation	-
Photoautotrophy	Ormerod	Phosphate	(100/20/∞)	NaHCO <sub>3</sub> (140)**	Light	Na <sub>2</sub> S (300)	CO <sub>2</sub>	-	No Na <sub>2</sub> S
Chemoheterotrophy	Ormerod	HEPES	100/10/2	Ethanol (60), Acetate (130)	Chemical	Organic	Acetate	With light	-
Inhibition of H <sub>2</sub>	DWW	-	100/12/4	DWW	Light	Organic	CO <sub>2</sub>	-	Acetate

	production	Ormerod d	Phosphat e	100/15/ $\infty$	(278) (600)	Acetate (600)	Light	Organic	CO <sub>2</sub>	-	(600) N limitatio n (1/10)
--	------------	--------------	---------------	------------------	----------------	------------------	-------	---------	-----------------	---	-------------------------------------

113 <sup>a</sup> Buffer systems: HEPES (5.9 g L<sup>-1</sup>), Phosphate (0.9 g K<sub>2</sub>HPO<sub>4</sub> + 0.66 g KH<sub>2</sub>PO<sub>4</sub>). <sup>\*\*</sup> mg C L<sup>-1</sup> <sup>\*\*\*</sup>  $\infty$  means in high excess due to buffering

## 114 **Hydrolysis and biomass decay**

115 Biomass (0.5 L) was collected from the PAnMBR reactor, which had the following characteristics: TSS  
 116 (2.8 g L<sup>-1</sup>), VSS (2.1 g L<sup>-1</sup>), TKN (0.079 g N L<sup>-1</sup>), TP (0.012 g P L<sup>-1</sup>), NH<sub>4</sub>-N (0 g N L<sup>-1</sup>), PO<sub>4</sub>-P (0.002 g P L<sup>-1</sup>)  
 117 and pH (7.22). The biomass was centrifuged in 50 mL Falcon tubes and the pellet redissolved again in  
 118 NaCl 0.2 M. This operation was repeated three times. Then, the biomass was dissolved in 0.5 L of  
 119 NaCl 0.2 M and was divided into two 0.25 L Schott bottles, which were subsequently flushed with N<sub>2</sub>  
 120 and magnetically stirred at 200 rpm. The bottles were operated for 30 d.

121 One of the bottles was covered with aluminium foil for ensuring dark conditions and was used for  
 122 the hydrolysis analysis. Liquid sampling was performed twice a week for analysing volatile fatty acids  
 123 (VFAs), NH<sub>4</sub>-N, PO<sub>4</sub>-P, total inorganic carbon (TIC) and pH. Headspace was analysed for CH<sub>4</sub>, H<sub>2</sub> and  
 124 CO<sub>2</sub>. TSS/VSS, TKN and TP was analysed every 7 d.

125 The other bottle was illuminated as indicated above and biomass samples were taken every 7 d for  
 126 analysing its specific activity, thus calculating the loss of activity due to biomass decay. Activity tests  
 127 were conducted by inoculating 10% v/v of biomass from the big bottle into triplicate 160 mL serum  
 128 bottles filled with Ormerod medium and buffered with phosphate buffer at pH 7.5. The experiments  
 129 were conducted under the same conditions than previously described for the analysis of the  
 130 heterotrophic growth. 100 mg COD L<sup>-1</sup> of acetate was used as the substrate and 10 mg NH<sub>4</sub>-N L<sup>-1</sup> was  
 131 supplemented as well. The specific phototrophic activity (SPA) was calculated as indicated below in g  
 132 COD g<sup>-1</sup> COD<sub>biomass</sub> d<sup>-1</sup>.

## 133 **Analytical methods**

134 TCOD and SCOD were determined by COD cell tests (Merck, 1.14541.0001, Darmstadt, Germany).  
 135 Dissolved NH<sub>4</sub>-N, NO<sub>2</sub>-N and PO<sub>4</sub>-P were determined by a QuikChem8000 Flow Injection Analyzer  
 136 (FIA) (Hach Company, Loveland, USA). Temperature and pH were measured using an Oakton pH 11  
 137 Series (Vernon Hill, IL, USA). TSS and VSS were determined by filtration according to standard  
 138 methods, where TSS were calculated after drying the sample in an oven at 105 ± 2 °C and VSS were  
 139 calculated after burning it in a furnace at 550 ± 5 °C (APHA. 1998). Illuminance (W m<sup>-2</sup>) was  
 140 measured with an IR light sensor (PAS Port<sup>TM</sup>, Roseville, CA, USA). VFA samples were analysed by gas  
 141 chromatography (Agilent Technologies 7890A GC System, Santa Clara, CA, USA) equipped with a  
 142 flame ionisation detector (GC/FID) and a polar capillary column (DB-FFAP). Gas samples were  
 143 analysed by GC (2014 Shimadzu, Kyoto, Japan) with thermal coupled detector (TCD) (Tait et al.

144 TKN and TP were determined using sulfuric acid, potassium sulfate and copper sulfate  
145 catalyst in a block digestor (Lachat BD-46, Hach Company, Loveland, CO, USA) (Patton and Truitt  
146 1992). TIC was analysed by using a total organic carbon (TOC) analyser (Shimadzu TOC-L CSH TOC  
147 Analyser with TNM-L TN unit) coupled to a near infrared detector (NIRD) for measuring the CO<sub>2</sub>. All  
148 soluble constituents were determined after filtering with a 0.45 µm membrane filter (Millipore,  
149 Millex®-HP, Merck Group, Darmstadt, Germany).

## 150 **Microbial characterization**

151 Biomass used for the metabolic analyses was characterized by pyrosequencing and fluorescence *in*  
152 *situ* hybridization (FISH). Details of these methods are provided on Supplementary Material.

## 153 **Statistical analysis**

### 154 **Data handling**

155 Biomass concentration was calculated in g VSS L<sup>-1</sup>, and it was further transformed into COD by using  
156 the COD relationship calculated from the biomass equation CH<sub>1.8</sub>O<sub>0.38</sub>N<sub>0.18</sub> (McKinlay and Harwood  
157 2010a) (1 g biomass expressed as VSS = 1.78 g COD).

158 The SPA were calculated by linear fitting of the first 4 points after 1 h of culturing (for avoiding *lag*  
159 *phase* interference) of the substrate time course and the substrate consumption rate was calculated  
160 as g COD (or C) L<sup>-1</sup> d<sup>-1</sup>. Then, volumetric rates were converted into specific rates by dividing into the  
161 biomass concentration (in g COD<sub>biomass</sub> L<sup>-1</sup>), thus the specific activities are given in g COD (or C) g<sup>-1</sup>  
162 COD<sub>biomass</sub> d<sup>-1</sup>.

163 Biomass yields ( $\gamma$ ) were calculated accounting for the initial and final biomass concentration (in g VSS  
164 L<sup>-1</sup>) based on substrate consumption. Biomass concentration was further transformed into COD and  
165 then yields are expressed as g COD<sub>biomass</sub> g<sup>-1</sup> COD.

### 166 **Parameters identification**

167 Results from batch experiments have been used for obtaining model parameters. These include  
168 single Monod parameters from heterotrophic (soluble substrates) and autotrophic growth  
169 (bicarbonate), as well as nutrient (N and P) limitation as a double Monod equation. The models are  
170 implemented in Aquasim 2.1d.

171 Parameter estimation has been performed in Aquasim 2.1d. The modified Aquasim has been used to  
172 determine the two-parameter uncertainty surface for specific uptake rate ( $k_M$ ) and saturation  
173 constant ( $K_s$ ) and simulate the substrate consumption of the batch tests. 95% Confidence intervals  
174 have been calculated by minimization of the residual sum of squares. The method for determining  
175 parameter estimation is described in (Batstone et al. 2003).

176 Biomass decay rate and hydrolysis first order parameters were calculated by non-linear regression  
177 using Aquasim 2.1d as indicated before. First order models were implemented in Aquasim, and data  
178 to fit was the SPA (for the decay rate) and organics, N, P and gas released (for hydrolysis).

179 **MODEL DESCRIPTION**

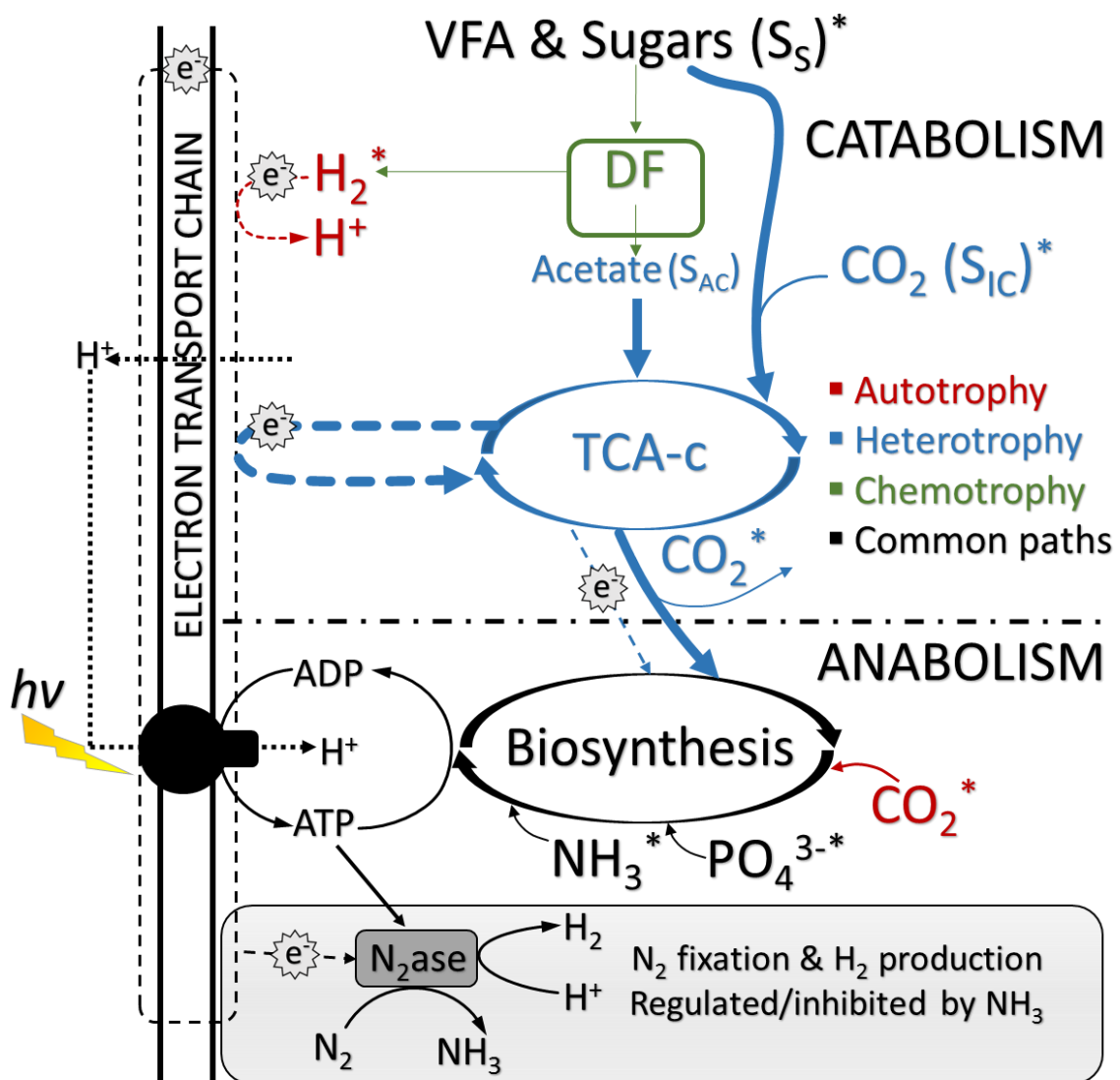
180 A novel mechanistic model has been developed for DWW treatment with nutrient recovery by PPB  
181 in anaerobic conditions. The units selected for the main components of the model have been g COD  
182 L<sup>-1</sup> (or Kg COD m<sup>-3</sup>) for both soluble and particulates as the ADM-1 model. Having the same units  
183 facilitates the link between partition by PPB and release by AD. Nutrient units were in g N L<sup>-1</sup> and g P  
184 L<sup>-1</sup>, respectively.

185 The kinetics and stoichiometry used in this model has been chosen as simply as possible. Monod  
186 kinetics has been selected for biological processes, whereas first order kinetics were used for  
187 biochemical mechanisms. Limiting conditions have been approached by using simple non-  
188 competitive equations. The complex metabolism of PPB has been simplified and only those  
189 processes relevant to DWW treatment has been included in the model. For this reason, only one  
190 biomass component has been selected (PPB), omitting the growth of other kind of biomass. It is,  
191 however, possible to upgrade the model by including other anaerobic biomass components, e.g.  
192 those described in the ADM-1. All the components and mechanistic processes has been detailed  
193 following matrix notation as the ASM and ADM-1 models.

194 This model is not addressing poly-P as well as other polymers accumulation, since it seems that PPB  
195 storage polymers in static (not growing) mode only (Hiraishi et al. 1991, Liang et al. 2010). The model  
196 is also omitting nitrification/denitrification processes since they can only occur in aerobic conditions  
197 where the NH<sub>4</sub><sup>+</sup> can be oxidized to nitrite or nitrate. Therefore, N and P are removed by assimilative  
198 growth only.

199 A schematic diagram of the model is presented in Figure 1. In presence of organic substrates,  
200 photoheterotrophy through the tri-carboxylic acids (TCA) cycle is preferred. Succinate coming from  
201 the TCA cycle gives electrons to the electron transport chain (ETC) through the succinate  
202 dehydrogenase. During growing mode or in presence of NH<sub>4</sub><sup>+</sup>, CO<sub>2</sub> is used as electron acceptor and  
203 enter into the Calvin Cycle. In static mode, H<sub>2</sub> production is inhibited by NH<sub>3</sub> presence. In absence of  
204 organic substrates, the biomass performs completely autotrophic growth using reduced inorganic  
205 compounds other than water for growing (anoxygenic photosynthesis). PPB can perform  
206 chemoheterotrophy at lower rate, providing H<sub>2</sub> to the photoautotrophy mechanism. (Golomysova et  
207 al. 2010, Gordon and McKinlay 2014, Klamt et al. 2008, Klamt et al. 2002, Koku et al. 2002, McKinlay

208 and Harwood 2010b). The scheme is not showing reductive power sources and electron flow  
 209 through the ETC for clarity purposes.



210

211 **Figure 1:** Schematic summary of PPB metabolism under domestic wastewater treatment. Key:  
 212 N2ase: Nitrogenase complex. TCA-c: Tri-carboxylic acid cycle. DF: Dark fermentation. VFA: volatile  
 213 fatty acids. e<sup>-</sup>: electrons. Dash: electron cycles. Dot: proton pumps. \*: Model compounds.

214 As the ASM models,  $S_?$  and  $X_?$  symbols are used for distinguishing between soluble and particulates,  
 215 respectively, where the subindex indicates the component type. A complete description of model  
 216 components can be accessed at Supplementary Information.

217 The processes described by this model are all based on PPB metabolism in anaerobic conditions.  
 218 Model mechanisms are described as follows:

- 219 (i) Photoheterotrophic metabolism on acetate (acetate uptake). It involves acetate  
220 assimilation by PPB for growing in light conditions. In dark conditions it will remain in the  
221 system, so it has been separated from the rest of photoheterotrophic metabolism. As a  
222 result of this process, CO<sub>2</sub> is excreted into the media.
- 223 (ii) Photoheterotrophic metabolism on other organics (photoheterotrophic uptake). These  
224 include all soluble organics that PPB can assimilate to growth in light conditions, as all  
225 the VFA's but acetate, some alcohols and some sugars. All of them are coalesced into  
226 one component. This process needs CO<sub>2</sub> assimilation as specified in Supplementary  
227 Information.
- 228 (iii) Chemoheterotrophic metabolism (chemoheterotrophic uptake). This mechanism  
229 involves the assimilative consumption of any organic in dark conditions that can be  
230 metabolized through either fermentation or anaerobic oxidation processes. All these  
231 processes have been joined as one mechanism for a shake of simplicity. This process  
232 involves H<sub>2</sub> and acetate as end products.
- 233 (iv) Photoautotrophic metabolism (autotrophic uptake). This mechanism involves the  
234 assimilative CO<sub>2</sub> fixation by PPB in light conditions using H<sub>2</sub> as the electron donor for the  
235 process. Other electron donors have been omitted but could be easily added to the  
236 model components, as Fe<sup>2+</sup>, S<sup>2-</sup> and S<sub>2</sub>O<sub>3</sub><sup>-</sup>.
- 237 (v) PPB cell decay (decay). This mechanism involves the deactivation of PPB by cell death.  
238 Ammonium, phosphate and inorganic carbon are released during this process and the  
239 biomass is converted into composites.
- 240 (vi) Hydrolysis and particulate fermentation (hydrolysis). The decomposition of particulates  
241 into organics ( $S_{Ac}$  and  $S_S$ ), ammonium, phosphate, hydrogen and inorganic carbon is  
242 addressed as a sole mechanism for simplicity. Both soluble and particulate inerts are  
243 also products of this process. A breakdown of particulate fermentation can be  
244 incorporate into the model according to the ADM-1 in particular cases (especially for  
245 long SRT processes).

246 The model is presented as Petersen matrix notation in Table 2. Complete set of rates and limiting  
247 factors are described in Supplementary Information.

248 **Table 2.** Petersen matrix of the PAM-1 model for domestic wastewater treatment by PPB.

<i>j</i>	Component ( <i>C</i> )	$\rightarrow$	<i>i</i>	1	2	3	4	5	6	7	8	9	10	
	Process↓		$S_S$	$S_{Ac}$	$S_{IC}$	$S_{h2}$	$S_{IN}$	$S_{IP}$	$S_I$	$X_{PB}$	$X_C$	$X_I$		
1	Hydrolysis/fermentation		$f_{ss,xc}$	$f_{SAc,xc}$	$f_{IC,xc}$	$f_{h2,xc}$	$f_{IN,xc}$	$f_{IP,xc}$	$f_{Si,xc}$	0	-1	$f_{xi,xc}$	Particulate inert (g COD L <sup>-1</sup> )	
2	Acetate uptake		0	-1	$f_{IC,ph,ac}$	0	- $f_{N,B}Y_{PB,ph}$	- $f_{P,B}Y_{PB,ph}$	0	$Y_{PB,ph}$	0	0	Composite biomass (g COD L <sup>-1</sup> )	
3	Photoheterotrophic uptake		-1	0	$f_{IC,ph,Ss}$	0	- $f_{N,B}Y_{PB,ph}$	- $f_{P,B}Y_{PB,ph}$	0	$Y_{PB,ph}$	0	0	Phototrophic biomass (g COD L <sup>-1</sup> )	
4	Chemoheterotrophic uptake		-1	$(1 - Y_{PB,ch})$ $f_{ac,ch}$	0	$(1 - Y_{PB,ch}) f_{h2,ch}$	- $f_{N,B}Y_{PB,ch}$	- $f_{P,B}Y_{PB,ch}$	0	$Y_{PB,ch}$	0	0	Soluble inert (g COD L <sup>-1</sup> )	
5	Autotrophic uptake		0	0	$f_{IC,a}$	$f_{h2,a}$	- $f_{N,B}Y_{PB,a}$	- $f_{P,B}Y_{PB,a}$	0	$Y_{PB,a}$	0	0	Inorganic phosphorous (g P <sub>2</sub> PO <sub>4</sub> L <sup>-1</sup> )	
6	Decay of XPB		0	0			0			0	-1	1	0	Inorganic nitrogen (g N-NH <sub>4</sub> L <sup>-1</sup> )
							$H_2$ (g COD L <sup>-1</sup> )							Soluble substrate (g COD L <sup>-1</sup> )
								$Inorganic\ carbon\ (mg\ C-HCO_3\ L^{-1})$						Acetate (g COD L <sup>-1</sup> )
														Soluble substrate (g COD L <sup>-1</sup> )

250 The kinetic parameters have been obtained from the experimental approach described later on in  
251 this work. Additional kinetic parameters included in the model are the saturation constant for  
252 hydrogen consumption by photoautotrophic process ( $K_{S,h2}$ ) light limitation ( $K_{S,E}$ ) and inhibition by  
253 ammonia ( $K_{I,FA}$ ). The parameters set are depicted in Supplementary Information.

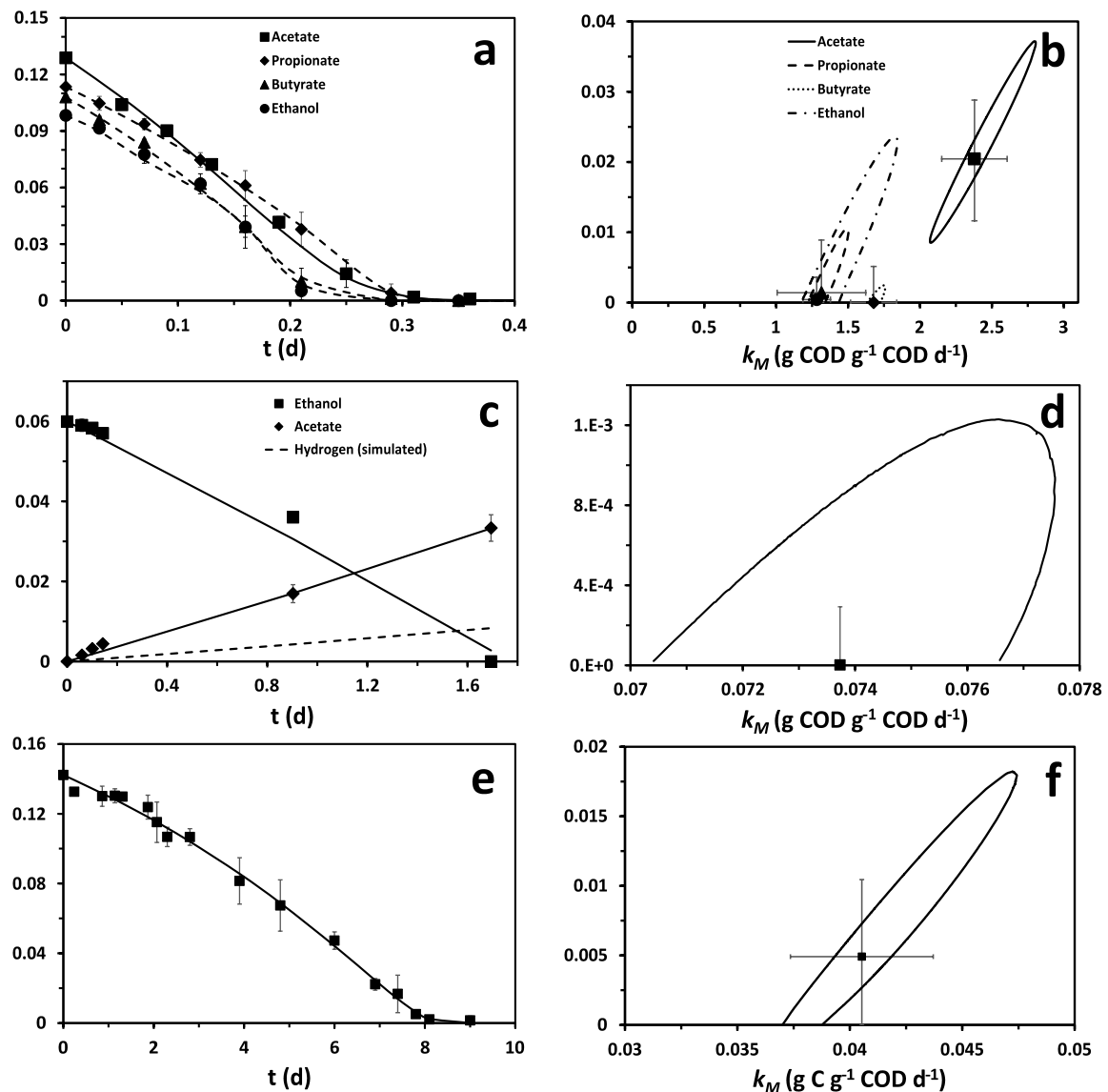
254 The stoichiometry of all the processes detailed above has been established by using the parameters  
255 determined experimentally, as well as by theoretical calculations based on the literature.  
256 Conservation equations have been used for closing balances as established in ASM models(Henze et  
257 al. 2006). The model is balanced in COD, C, N and P.  $\text{HCO}_3^-$ ,  $\text{NH}_4^+$  and  $\text{PO}_4^{2-}$  have been used for closing  
258 C, N and P balances, respectively. A detailed explanation for stoichiometric calculations and  
259 derivations is found in Supplementary Information, as well as the stoichiometric parameters values  
260 before and after computed for conservation

## 261 **Mechanisms of the model**

262 The sludge used for all the experiments that came from the lab-scale PAnMBR has been  
263 microbiologically characterized through pyrosequencing as well as by FISH. Most of the  
264 microorganisms are related with  $\alpha$ -proteobacteria, as detected by FISH (Supplementary  
265 Information). The sludge is clearly dominated by PPB microorganisms, accounting for more than 70%  
266 of the total gene copies detected by the pyrosequencing technique (see Supplementary  
267 Information). The genus *Rhodobacter* ssp. is the most represented in the microbiota with more than  
268 60%. The presence of other phototrophs as microalgae and cyanobacteria is residual, with less than  
269 1% of total gene copies. Therefore, the biomass can be considered as PPB-dominant biomass, which  
270 all the light processes being carried out by PPB exclusively.

271 The mechanisms of photoheterotrophy by PPB were analysed by using VFAs and ethanol. All the  
272 substrates were completely consumed in the experimental time (Figure 2a), and the growing  
273 efficiency was in all cases similar, since the average biomass yield was calculated to be  $1.19 \pm 0.03$  g  
274  $\text{COD}_{\text{biomass}} \text{ g}^{-1}$  COD at a 95% confidence level. However, the acetate uptake mechanism should be  
275 differentiated from the mechanism of other organics uptake (propionate, butyrate and ethanol),  
276 since kinetic parameters are statistically different at 95% confidence (Figure 2b).

277



278

279 **Figure 2:** Experimental (symbols) and modelled (lines) time curse of substrates uptake (left) and  
 280 parameters determination including 95% confidence intervals and confidence regions (right) of PPB  
 281 metabolism in photoheterotrophy (a), chemoheterotrophy (b) and photoautotrophy (c) growth  
 282 modes.

283 Two major mechanisms of electron disposing by PPB are considered. Production of  $\text{CO}_2$  is a key  
 284 feature of PPB biomass at growing conditions (McKinlay and Harwood 2010a) and is important for  
 285 closing the C balance. The oxidation state of the organic compound determines if the biomass needs  
 286  $\text{CO}_2$  for substrate uptake (reduced substrates like propionate, butyrate or valerate), or the uptake  
 287 produces  $\text{CO}_2$  (oxidized substrates like acetate, succinate or ethanol)(McKinlay and Harwood 2011).  
 288 In this later case, the biomass disposes the excess of electrons in growing conditions by re-fixing the  
 289  $\text{CO}_2$  produced in the TCA cycle. As a consequence the total balance of  $\text{CO}_2$  in the system remains  
 290 close to neutrality. A theoretical explanation of this mechanism is explained in Supplementary

Information. The other major mechanism of electron disposing by PPB is the H<sub>2</sub> production via Nitrogenase complex. In static mode, the PPB biomass is able to use the excess of electrons for redox balance at the end of the ETC (see Figure 1). The ferredoxin complex is the carrier for this process, but the biomass need energy in form of ATP. However, this process has been claimed to be inhibited in presence of NH<sub>4</sub><sup>+</sup>, a strong inhibitor of the nitrogenase activity (Li et al. 2010, Rodionov et al. 1986). Indeed, this process has been studied and demonstrated that H<sub>2</sub> production is inhibited in a DWW fed situation due to (i) presence of ammonium and (ii) disposing of electrons by CO<sub>2</sub> re-fixation that promotes the growth (see Supplementary Information for more details). Therefore, it can be deduced that CO<sub>2</sub> production and re-fixation into de Calvin Cycle is the major electron sink in the PPB metabolism treating DWW.

Analysis of chemoheterotrophic metabolism by PPB was conducted by using acetate and ethanol as substrates in dark conditions (Figure 2c). PPB biomass was much less effective in dark conditions rather than in light conditions (biomass yielded 0.5 vs 1.1 g COD<sub>biomass</sub> g<sup>-1</sup> COD in dark and light conditions, respectively). Also the Monod parameters, calculated by using the stoichiometry of the anaerobic syntrophic ethanol oxidation to acetate (Seitz et al. 1990), showed a much lower kinetics of the chemotrophic metabolism compared to photoheterotrophy (Figure 2d). Despite chemotrophic processes are residual, they must be considered in a DWW situation for closing COD, C and nutrient balances. Acetate is the end product of these processes and can be only used by PPB in light conditions due to absence of high concentrations of oxidized lithotrophic substrates, as Fe(III)(Finneran et al. 2003).

The analysis of the photoautotrophic metabolism of PPB was conducted by using NaHCO<sub>3</sub> as C source and Na<sub>2</sub>S as electron donor for the process in 5-fold stoichiometric excess (see Table 1), thus knowing the theoretical maximum uptake rate of inorganic carbon (IC) by PPB (Figure 2e). The biomass was efficient on autotrophic growth, having a biomass yield of 3.0 g COD<sub>biomass</sub> g<sup>-1</sup> IC that is comparable to the value on acetate (4 g COD<sub>biomass</sub> g<sup>-1</sup> C). However, the autotrophic kinetics was much slower than the heterotrophic, as can be seen in Figure 2f. As in the case of the chemoheterotrophy, the mechanism of photoautotrophy need to be considered for closing the COD, C and nutrient balances.

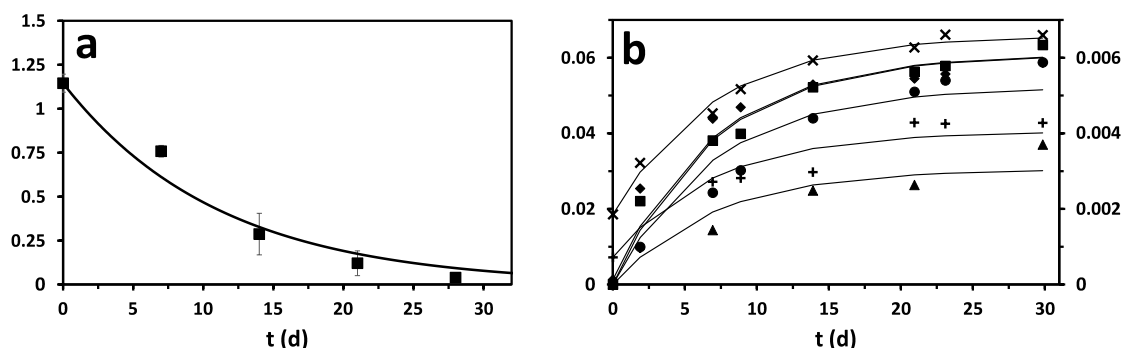
The effect of nutrient limitation on the PPB growth kinetics has been also explored for calculating the saturation constant for nutrients removal. An experiment has been conducted by using low N and P concentrations as indicated in Table 1. A double-Monod growth model including COD and N or P growth limitation has been used and saturation constants for N and P has been calculated. Main results are included in Supplementary Information. Very low K<sub>s</sub> values convert N and P into switch

324 functions. Biomass assimilated nutrients at a COD/N/P ratio of 100/7.1/1.8. However, PPB was able  
 325 to grow at lower rate once the nutrients have been completely consumed. PPB metabolism can  
 326 fixate atmospheric N<sub>2</sub> after ammonium depletion(Hunter et al. 2008). This process has been proved  
 327 to be inhibited by ammonium. Also, PPB can accumulate polymers like poly-phosphate (Liang et al.  
 328 2010) as well as PHA (Melnicki et al. 2009), which can be used in static mode for growing. This  
 329 phenomenon is typical in batch conditions but in steady-state continuous growth P is mainly used  
 330 for growing and is not bioaccumulated (Hulsen et al., 2015 REF-CONTINUOUS PAPER). Therefore  
 331 nutrient switch functions have to be considered.

332 Hydrolysis and biomass decay were considered as transversal biochemical mechanisms. Both  
 333 processes have been included previously in most of the kinetic models applied for wastewater  
 334 treatment (Batstone et al. 2006, Henze et al. 2006, Szilveszter et al. 2010). The analysis of hydrolysis  
 335 and biomass decay PPB has been conducted as indicated in Table 1. The approach diverged for the  
 336 two mechanisms due to the particularity of PPB metabolism. The decay rate was analysed in full  
 337 illumination conditions for emulating a real case where the bacterial life-death cycle is occurring  
 338 during full-energy continuous operation. During the starvation period, biomass was dying and it was  
 339 traduced in a decrease of VSS and metabolic activity. Figure 3a shows the time course of the SPA  
 340 values (on acetate) calculated for the PPB biomass suffering the starvation. The biomass lost all the  
 341 activity in around 28 d. A first order model was applied for calculating the decay rate constant (0.09  
 342 ± 0.02 d<sup>-1</sup>). The analysis of hydrolysis was conducted in dark conditions, otherwise the compounds  
 343 released upon hydrolysis can be re-assimilated again by the still living PPB. The hydrolysis is anyway  
 344 independent from light. The release of organic (VFA's and ethanol) and inorganic (TIC, H<sub>2</sub>, NH<sub>4</sub><sup>+</sup> and  
 345 PO<sub>4</sub><sup>3-</sup>) compounds were analysed and fitted to a first order model (Figure 3b). The hydrolysis  
 346 constant has been calculated to be 0.071 ± 0.004 d<sup>-1</sup>. Fitting curves are depicted in Figure 3b as well.  
 347 The goodness of fitting indicates that first order kinetics explain very well both mechanisms.

348

349



350 **Figure 3:** Mechanism of decay rate (a) and hydrolysis (b). Time course of specific phototrophic  
351 activity of PPB subjected to starvation under full illumination (a), and time course of released  
352 products upon starvation in dark conditions: soluble organic compounds but acetate (squares),  
353 acetate (diamonds), hydrogen (triangles), TIC (pluses), NH<sub>4</sub><sup>+</sup>-N (circles) and PO<sub>4</sub><sup>3-</sup>-P (crosses) (b).

354 **Compare and contrast.**

355 Values for kinetic parameters have been compared to those reported in the literature for different  
356 species of PPB and mixed cultures. A full list of parameter values and statistical significance can be  
357 found in Supplementary Material, whereas Table 3 shows a brief descriptive statistical analysis of the  
358 values found in the literature for certain parameters in comparison with those reported here. Values  
359 were extracted and calculated assuming that: (i) protein composition of PPB is in all cases 60% of dry  
360 weight(McKinlay and Harwood 2010a), (ii) 1 g VSS = 1.78 g COD and (iii) PPB biomass equation is  
361 CH<sub>1.8</sub>O<sub>0.38</sub>N<sub>0.18</sub>(McKinlay and Harwood 2010a). A difference between the arithmetic (average) and  
362 geometric means is found when the data is not following normal distribution. The heterogeneity of  
363 the parameter values lead to perform the statistical comparison from a physiological and  
364 mechanistic point of view rather than quantitatively.

365 In general, biomass yields calculated here are well in line with values reported in the literature. The  
366 only exception is the biomass yield for autotrophic growth. Several authors reported values much  
367 higher than the value reported here ( $3.0 \pm 0.2$  g COD g<sup>-1</sup> C fixed), which anyway is very close to the  
368 theoretical maximum yield for carbon dioxide fixation of (3.32 g COD g<sup>-1</sup> C). The media composition  
369 in these studies contained carbonaceous compounds other than HCO<sub>3</sub><sup>-</sup>, so (i) CO<sub>2</sub> fixation could be  
370 promoted in the assimilation of reduced organic substrates(McKinlay and Harwood 2011), and (ii)  
371 PPB biomass would assimilate these substrates heterotrophically, in both cases increasing  
372 substantially the biomass yield.

373 However, specific uptake rates somehow diverged substantially. Certain studies were focused on the  
374 analysis of a specific metabolic mechanism and, with this purpose, the biomass was enriched in  
375 optimum conditions. A clarifying example is found in (Schultz and Weaver 1982) where the growth  
376 rates of *Rhodospirillum rubrum* and *Rhodopseudomonas capsulata* were studied on several  
377 chemoheterotrophic substrates in the dark. The authors used trimethylamine-N-oxide as accessory  
378 oxidant to promote the fermentation and anaerobic oxidation of fructose, glucose and succinate by  
379 PPB, which must increase the specific uptake rate of these compounds. Also, photoheterotrophic  
380 uptake rates have been traditionally obtained in hydrogen production processes. Under these  
381 situations, the substrate uptake is optimized for biogenic H<sub>2</sub> by dislocating catabolism from

382 anabolism, considerably increasing the substrate uptake rate while maintaining constant the  
 383 biomass growth(Basak and Das 2007). In addition, pure culturing (the most of parameters reported  
 384 in Table 3) promotes specific uptake rates in decrement of substrate affinity, which lets to increased  
 385  $k_M$  and  $K_S$  parameters, a typical behaviour of r-strategist microorganisms (Dorodnikov et al. 2009).

386 Hydrolysis and decay rates are very dependent on the oxidizing conditions of the process. In  
 387 general, the more oxidizing the system is, the faster the biomass decay and, consequently, faster  
 388 hydrolysis as well (REF) (although the anaerobic digestion processes are an exception). The biomass  
 389 decay and hydrolysis constants found in the literature were obtained in aerobic photoheterotrophic  
 390 processes (Huang et al. 1999, Huang et al. 2001), which explains that they are considerably higher  
 391 than those calculated here.

392 In definitive, the kinetic parameters obtained in this study serve for characterising mechanistically  
 393 the biomass extracted from the PAnMBR process. This biomass is defined by a dominance of the  
 394 photoheterotrophic metabolism with some reminiscences of other metabolic mechanisms. The  
 395 biomass seems to be clearly K-strategist which promotes the substrate affinity instead of the uptake  
 396 by minimizing the affinity constants ( $K_S$ ), a microbial strategy in low-strength systems as domestic  
 397 wastewater with low hydraulic retention times (less than 12 h) which is useful for over-competing  
 398 other microorganisms (Dorodnikov et al. 2009).

399 **Table 3:** Statistical comparison of estimated parameters with those reported in the literature.

	$k_{M,ac}$	$k_{M,ph}$	$k_{M,ch}$	$k_{M,ic}$	$K_{S,s}$	$Y_{PB,ph}$	$Y_{PB,ch}$	$Y_{PB,a}$	$k_{hyd}$	$k_{dec}$
	g COD g <sup>-1</sup> COD d <sup>-1</sup>	g COD g <sup>-1</sup> COD d <sup>-1</sup>	g COD g <sup>-1</sup> COD d <sup>-1</sup>	g IC g <sup>-1</sup> COD d <sup>-1</sup>	mg COD L <sup>-1</sup>	g COD g <sup>-1</sup> COD	g COD g <sup>-1</sup> COD	g COD g <sup>-1</sup> g <sup>-1</sup> C	d <sup>-1</sup>	d <sup>-1</sup>
Calculated	2.4	1.4	0.074	0.041	0.524	1.2	0.5	3	0.07	0.09
Average	1.5	11	5	0.3	4333	0.78	0.23	11	0.27	0.20
Geometric mean	1.4	5	3	0.2	749	0.68	0.21	9	0.27	0.20
Standard deviation	0.5	13	4	0.2	6036	0.37	0.12	7	0.06	0.02
N samples	2	12	8	9	2	17	8	4	2	2
Confidence 95%	4.6	8	3	0.1	54228	0.18	0.10	11	0.58	0.21
References	1	2	3	4	5	6	7	8	9	10

400 <sup>1</sup>(Golomysova et al. 2010, McKinlay and Harwood 2011), <sup>2</sup>(Gadhamshetty et al. 2008, Golomysova  
 401 et al. 2010, Klein et al. 1991, McKinlay and Harwood 2011, Obeid et al. 2009), <sup>3</sup>(Madigan and Gest  
 402 1978, Schultz and Weaver 1982), <sup>4</sup>(Sarles and Tabita 1983, Wang et al. 1993), <sup>5</sup>(Gadhamshetty et al.  
 403 2008, Obeid et al. 2009), <sup>6</sup>(Gadhamshetty et al. 2008, Klamt et al. 2002, Klein et al. 1991, McKinlay

404 and Harwood 2011, Obeid et al. 2009, Schultz and Weaver 1982),<sup>7</sup> (Madigan and Gest 1978, Schultz  
405 and Weaver 1982),<sup>8</sup> (Wang et al. 1993),<sup>9</sup> (Huang et al. 1999, Huang et al. 2001),<sup>10</sup> (Huang et al.  
406 1999, Huang et al. 2001)

#### 407 **Implications of the model. Simulations under specific scenarios.**

408 The model has been tested for exploring different scenarios and then knowing limits of the process  
409 as well as possible adaptations of the model by biomass shifts on metabolism. The model has been  
410 implemented in Matlab R2014a, where the simulations have been performed. Detailed information  
411 about the simulations is provided in **Supplementary Information**.

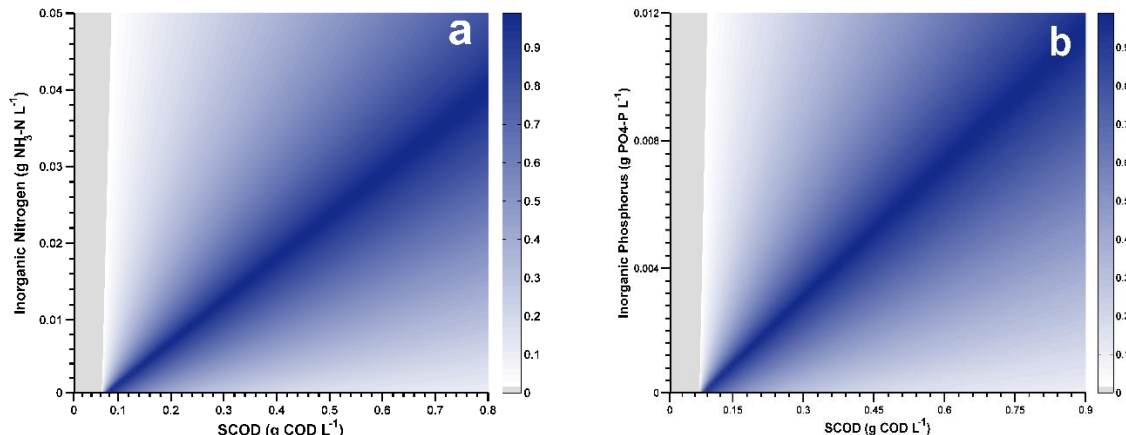
#### 412 **Scenario 1. Domestic wastewater with deficiency of C or nutrients (N and P)**

413 In this scenario the main metabolic pathway to be analysed is the photoheterotrophic metabolism.  
414 Since the main outcome of the PRR concept is the complete assimilation of C, N and P by PPB, it is  
415 necessary to explore the limits of the process in terms of optimum COD/N/P conditions for typical  
416 DWW treatment systems.

417 Systematic (not-random) simulations have been performed with the main fixed components:  
418 biomass concentration (0.05 g COD L<sup>-1</sup>), no light limitation and experimental time (2.5 d). More  
419 details are found in **Supplementary Information**. Variable conditions were soluble substrate (0.01-0.5  
420 g COD L<sup>-1</sup>), acetate (0.01 – 0.5 g COD L<sup>-1</sup>), ammonium (0.005-0.065 g N L<sup>-1</sup>) and phosphate (0.001-  
421 0.015 g P L<sup>-1</sup>). A total of 2 sets of 50x50 simulations were performed by varying (i) SCOD and  
422 ammonium, and (ii) SCOD and phosphate. Figure 4 shows the results of the simulations. X-axis  
423 represents the initial concentration of the sum of all soluble substrates, whereas Y-axis are the initial  
424 NH<sub>4</sub><sup>+</sup>-N and PO<sub>4</sub><sup>2-</sup>-P concentration for Figures 4a and 4b, respectively. Values in the graphs  
425 represents normalized uptake efficiencies where 1.0 represents 100% removal of both soluble  
426 substrate and the respective nutrient. Values lower than 1.0 represent that one of the varying  
427 components is not fully consumed.

428 Optimum COD/N/P relationship has been calculated to be 100/7.1/1.8. According to Figure 4, there  
429 is three possible regions outside the optimum in a real case: (i) low nutrients concentration where  
430 there is a net accumulation of the SCOD in the system –overload- (ii) high nutrients concentration  
431 where all the SCOD is consumed but the effluents still contains N and P –underload-, and (iii) very  
432 low COD that is never going to be enough for maintaining biomass growth despite nutrients  
433 concentration. Region (iii) is the only that cannot be sustained in a long-term process due to biomass  
434 decay. Region (i) is not possible in a DWW scenario where nutrients are always in excess. It could be  
435 the case for other kind of wastewaters. Respect to the region (ii), that is the most typical case, it is

436 clear that the only way of obtaining full nutrient removal is by adding external SCOD to the system.  
437 Figure 4 could serve as a quick guide for estimating the need for treatment in a real case.



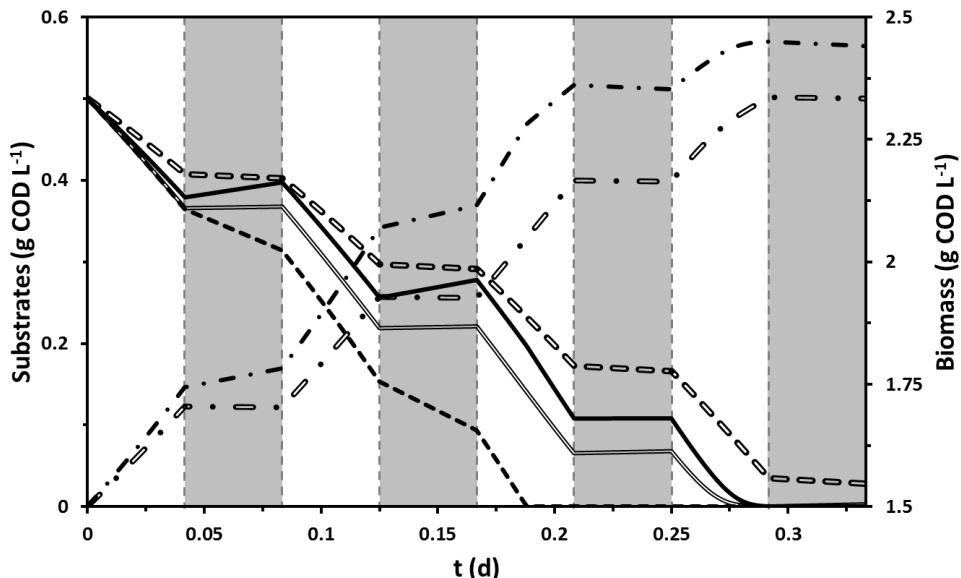
438  
439 **Figure 4.** Normalized efficiency of SCOD and  $\text{NH}_4^+$ -N (a) or  $\text{PO}_4^{2-}$ -P (b) removal by PPB in a simulated  
440 scenario at different SCOD/N/P ratios, where maximum efficiency (1.0, dark blue) corresponds to  
441 total consumption of SCOD and nutrients. Grey area represents negative efficiencies, where the  
442 biomass decay is higher than growth and therefore is not sustainable.

#### 443 **Scenario 2. Effect of chemoheterotrophic processes in light-limiting conditions 444 during light/dark cycles.**

445 Parameters calculated in this work are conditioned by the origin of the biomass. The PAnMBR  
446 reactor was operated at full illumination with no light/dark cycles. Although this is the normal  
447 operation procedure for PPB, in some cases artificial illumination could be avoided by using natural  
448 sun light as energy source as happen usually with algae reactors (Christenson and Sims 2011). During  
449 dark (night) cycles, the biomass need to make use of an energy source other than light so it is  
450 predictable that the metabolism would shift into mixed photo-chemoheterotrophy. Indeed, several  
451 authors have published that PPB are able to follow chemoheterotrophic metabolism achieving  
452 substrate uptakes rates at least one order of magnitude above the values calculated here (see Table  
453 3). Therefore, it is necessary to explore how the system behaves under a promoted  
454 chemoheterotrophy during light/dark cycles.

455 A set of two simulations were performed by including light/dark cycles (1 h each for a total of 6  
456 cycles) during a typical batch test scenario where all the conditions were fixed but the uptake rate  
457 for chemoheterotrophic metabolism was modified using two different values ( $k_{M, ch} = 0.074$  and  $0.7 \text{ g}$   
458  $\text{COD g}^{-1} \text{ COD d}^{-1}$ ). Conditions and rationality for the simulation are described in **Supplementary**  
459 **Information**. Results from the simulation are depicted in Figure 5. As can be seen, when the biomass  
460 have a high chemoheterotrophic activity, soluble substrate is consumed giving rise to acetate

461 accumulation that is eventually consumed during light cycles. A net production of hydrogen happen  
 462 due to fermentation/anaerobic oxidation processes, which can be used for promoting autotrophic  
 463 growth. This can be also connotations on the possible biomass shift to autotrophic metabolism, as  
 464 will be discussed later. Since the biomass yield is lower during chemoheterotrophic metabolism,  
 465 there is a lower net increase of biomass.



466

467 **Figure 5.** Effect of dark/light cycles on PPB metabolism under low (double lines) and high (single  
 468 lines) chemoheterotrophic activity ( $k_{M, ch} = 0.074$  and  $0.7 \text{ g COD g}^{-1} \text{ COD d}^{-1}$ , respectively). Simulation  
 469 of the time course of acetate (continuous line), ethanol (dash line) and biomass (dash-dot lines)  
 470 concentrations during 1 h dark/light periods.

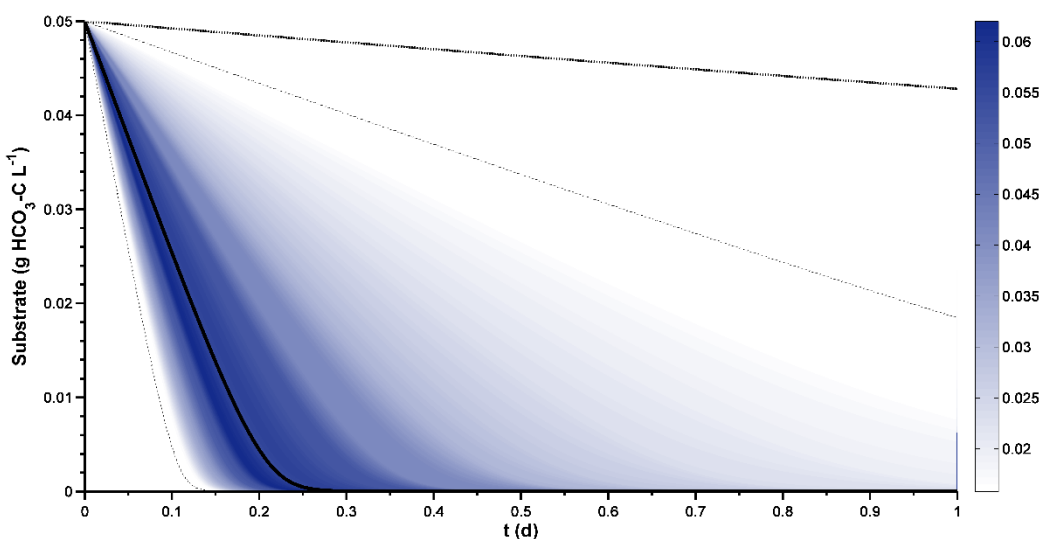
471

### 472 **Scenario 3. Promotion of carbon dioxide fixation in DWW coming from hard 473 waters.**

474 In this scenario the promotion of autotrophy is discussed and the autotrophic metabolism is  
 475 analysed. The DWW used for the batch experiments and for the continuous PAnMBR came from a  
 476 DWW collector located in Brisbane (Australia). Water in this place can be considered as moderately  
 477 hard (hardness =  $148 \pm 7 \text{ mg CaCO}_3 \text{ L}^{-1}$ , n=19, which corresponds to  $53 \text{ mg C L}^{-1}$ ). Therefore, there is a  
 478 clear potential to enrich the PPB process in autotrophic conditions. However, this is only possible if  
 479 there is an electron donor for the process, mainly  $\text{Fe}^{2+}$ ,  $\text{S}^{2-}$  or  $\text{H}_2$ (Hunter et al. 2008), or reduced  
 480 organics(McKinlay and Harwood 2011). The promotion of reductive processes as fermentation or  
 481 anaerobic oxidation (including sulfate reduction as well) could give risen to the reduced components

482 for carbon dioxide fixation to be feasible. This analysis is focused on the results after the reduced  
483 conditions appeared, so the discussion on how these conditions are possible is out of scope.

484 A simulation has been conducted to analyse how the model behaves on a promoted autotrophic  
485 metabolism scenario. To that purpose, the initial conditions have been fixed and only the H<sub>2</sub>  
486 concentration has been increased to 0.175 g COD L<sup>-1</sup> to cope with the stoichiometric requirements of  
487 autotrophic carbon dioxide fixation. Then, the simulation has been performed by using the  
488 autotrophic uptake rate value calculated here ( $k_{M,ic}=0.041$  g C g<sup>-1</sup> COD d<sup>-1</sup>) and a Gaussian-random  
489 set of 500 Montecarlo simulations using the average and 95% confidence intervals for the  $k_{M,au}$   
490 values reported in the literature (as reported in Table 3). Simulation conditions and rationality are  
491 described in [Supplementary Material](#). The results are depicted in Figure 6. As can be seen, the  
492 autotrophic process using the calculated values seems to be residual compared to the  
493 photoheterotrophic metabolism. However, the autotrophic promotion can modify substantially the  
494 scenario. In the most probable case (using the mean of the  $k_{M,ic}$  from Table 3), the biomass is able to  
495 fix 1 g TIC L<sup>-1</sup> in the same time than they assimilate 1.76 g C L<sup>-1</sup> by the photoheterotrophic  
496 metabolism. Therefore, the carbon dioxide fixation could become a major process, which potentially  
497 could account for around 36% of N and P removal.



498  
499 **Figure 6.** Photoautotrophic-promoted metabolism behaviour. Time course of inorganic carbon for  
500  $k_{M,ic}$  values obtained by a Gaussian-random set of Montecarlo simulations based on literature  
501 reported values for phototrophic bacteria (blue shades), including the simulation using the mean  
502 (continuous line) and 95% confidence intervals of the mean (short dot-points). It is also shown the  
503 simulation using the parameter value determined in the present paper (dot line).

504 **Recommendations, limitations and future work.**

505 This study presents the first model for domestic wastewater treatment by purple phototrophic  
506 bacteria, under the scope of the new platform proposed for domestic wastewater treatment, the  
507 Partition-Release-Recovery concept, developed by (Batstone et al. 2014), and funded by the CRC for  
508 Water Sensitive Cities Program and the Smart Water Fund. The model will serve as a basis for the  
509 implementation of the technology in DWW treatment in Australia, as a first step, and then to spread  
510 the technology overseas.

511 The model has described the following implications that can be used as recommendations for up-  
512 scaling:

- 513 (i) The PPB process in DWW fed situation performs mainly through photoheterotrophic  
514 metabolism. Maximum uptake rate is between  $1.4\text{--}2.4 \text{ g COD g}^{-1} \text{ COD d}^{-1}$  with a biomass  
515 yield of around  $1 \text{ g COD g}^{-1} \text{ COD}$ . For a typical wastewater treatment plant, with a solid  
516 retention time of 2 d and a TCOD of  $1 \text{ g L}^{-1}$ , it involves a **minimum HRT of 5.7 h**.
- 517 (ii) It is necessary to provide extra addition of SCOD to the system to cope with full nutrient  
518 removal. The extra addition will depends on the wastewater composition, according to  
519 the COD/N/P ratio of 100/7.1/1.8.
- 520 (iii) The chemoheterotrophic behaviour of the PPB biomass is very dependent on the DWW  
521 composition. It is recommended to study in detail this process in each particular case,  
522 especially in systems designed with light/dark cycles.

523 The model has the following limitations:

- 524 (i) This model is for domestic wastewater treatment only. It is not recommended to use for  
525 any other kind of wastewater without the necessary modifications.
- 526 (ii) The model is only valid for anaerobic conditions, and hydrogen production for redox  
527 balancing is assumed to be inhibited, so this model cannot be implemented for  
528 hydrogen production systems as it is.
- 529 (iii) The model is not contemplating poly-P as well as other polymers accumulation. Also,  
530 nitrogen fixation is not included since it is assumed to be inhibited by ammonium.
- 531 (iv) This model represents a simplification of PPB metabolism, and includes biological  
532 mechanisms only. Implementation in full case needs to include hydrodynamics, light  
533 harvesting, gas phase addition, ionic charges and pH simulation. An update of the model  
534 is currently ongoing and will be implemented in a real Pilot-plant set-up.

535 Future work will include the upgrading of the model to cope with the limitations. Specifically, we  
536 are currently addressing poly-P and PHA accumulation as well as N<sub>2</sub> fixation and side H<sub>2</sub> production.  
537 The effect of specific components/characteristics of wastewater other than domestic are also being  
538 addressed (as typical heavy metals –Cu and Zn-, low and high pH and their combined effect with  
539 ammonium and free ammonia, and components of specific wastewaters as pharmacs, hormones,  
540 aromatic volatiles or biocides, among others).

## 541 **ACKNOWLEDGEMENTS**

542 This work was jointly funded by the Smart Water Fund (project 10OS-023) and the CRC for Water  
543 Sensitive Cities (project C2.1). Thanks are given to Prof. James B. McKinlay for his kind discussion on  
544 PPB metabolism.

## 545 **REFERENCES**

- 546 APHA. (1998) Standard Methods for the Examination of Water and Wastewater. 20th ed. American  
547 Public Health Association, Washington, DC, USA.  
548 Basak, N. and Das, D. (2007) The prospect of purple non-sulfur (PNS) photosynthetic bacteria for  
549 hydrogen production: the present state of the art. World Journal of Microbiology and Biotechnology  
550 23(1), 31-42.  
551 Batstone, D.J., Hülsen, T., Mehta, C.M. and Keller, J. (2014) Platforms for energy and nutrient  
552 recovery from domestic wastewater: A review. Chemosphere (0).  
553 Batstone, D.J., Keller, J., Angelidaki, I., Kalyuzhnyi, S., Pavlostathis, S., Rozzi, A., Sanders, W., Siegrist,  
554 H. and Vavilin, V. (2002) The IWA Anaerobic Digestion Model No 1(ADM 1). Water Science &  
555 Technology 45(10), 65-73.  
556 Batstone, D.J., Keller, J. and Steyer, J. (2006) A review of ADM 1 extensions, applications, and  
557 analysis: 2002-2005. Water Science and Technology 54(4), 1-10.  
558 Batstone, D.J., Pind, P.F. and Angelidaki, I. (2003) Kinetics of thermophilic, anaerobic oxidation of  
559 straight and branched chain butyrate and valerate. Biotechnol Bioeng 84(2), 195-204.  
560 Brandl, H., Gross, R.A., Lenz, R.W., Lloyd, R. and Fuller, R.C. (1991) The accumulation of poly(3-  
561 hydroxyalkanoates) in Rhodobacter sphaeroides. Archives of Microbiology 155(4), 337-340.  
562 Christenson, L. and Sims, R. (2011) Production and harvesting of microalgae for wastewater  
563 treatment, biofuels, and bioproducts. Biotechnology Advances 29(6), 686-702.  
564 Dorodnikov, M., Blagodatskaya, E., Blagodatsky, S., Fangmeier, A. and Kuzyakov, Y. (2009)  
565 Stimulation of r- vs. K-selected microorganisms by elevated atmospheric CO<sub>2</sub> depends on soil  
566 aggregate size: Research article. FEMS Microbiology Ecology 69(1), 43-52.  
567 Eroglu, I. (2008) Hydrogen production by Rhodobacter sphaeroides O.U.001 in a flat plate solar  
568 bioreactor. International Journal of Hydrogen Energy 33(2), 531-541.  
569 Fang, H.H.P., Liu, H. and Zhang, T. (2005) Phototrophic hydrogen production from acetate and  
570 butyrate in wastewater. International Journal of Hydrogen Energy 30(7), 785-793.  
571 Finneran, K.T., Johnsen, C.V. and Lovley, D.R. (2003) *Rhodoferax ferrireducens* sp. nov., a  
572 psychrotolerant, facultatively anaerobic bacterium that oxidizes acetate with the reduction of Fe(III).  
573 International Journal of Systematic and Evolutionary Microbiology 53(3), 669-673.  
574 Gadhamshetty, V., Sukumaran, A., Nirmalakhandan, N. and Theinmyint, M. (2008)  
575 Photofermentation of malate for biohydrogen production— A modeling approach. International  
576 Journal of Hydrogen Energy 33(9), 2138-2146.

- 577 Golomysova, A., Gomelsky, M. and Ivanov, P.S. (2010) Flux balance analysis of photoheterotrophic  
578 growth of purple nonsulfur bacteria relevant to biohydrogen production. International Journal of  
579 Hydrogen Energy 35(23), 12751-12760.
- 580 Gordon, G.C. and McKinlay, J.B. (2014) Calvin cycle mutants of photoheterotrophic purple nonsulfur  
581 bacteria fail to grow due to an electron imbalance rather than toxic metabolite accumulation. J  
582 Bacteriol 196(6), 1231-1237.
- 583 Henze, M., Gujer, W., Mino, T. and Van Loosdrecht, M. (2006) Activated sludge models ASM1,  
584 ASM2, ASM2d and ASM3.
- 585 Hiraishi, A., Yanase, A. and Kitamura, H. (1991) Polyphosphate Accumulation by *Rhodobacter*  
586 *sphaeroides* Grown under Different Environmental Conditions with Special Emphasis on the  
587 Effect of External Phosphate Concentrations. Bulletin of Japanese Society of Microbial Ecology 6(1),  
588 25-32.
- 589 Huang, J.S., Jih, C.G. and Sung, T.J. (1999) Performance enhancement of suspended-growth reactors  
590 with phototrophs. Journal of Environmental Engineering 125(6), 501-507.
- 591 Huang, J.S., Wu, C.S., Jih, C.G. and Chen, C.T. (2001) Effect of addition of *Rhodobacter* sp. to  
592 activated-sludge reactors treating piggery wastewater. Water Res 35(16), 3867-3875.
- 593 Hulsen, T., Batstone, D.J. and Keller, J. (2014) Phototrophic bacteria for nutrient recovery from  
594 domestic wastewater. Water Res 50, 18-26.
- 595 Hulsen, T., Batstone, D.J. and Keller, J. (2014) Phototrophic bacteria for nutrient recovery from  
596 domestic wastewater. Water Research 50, 18-26.
- 597 Hunter, C.N., Daldal, F., Thurnauer, M.C. and Beatty, J.T. (2008) The Purple Phototrophic Bacteria,  
598 Springer.
- 599 Jetten, M.S.M., Horn, S.J. and van Loosdrecht, M.C.M. (1997) Towards a more sustainable municipal  
600 wastewater treatment system. Water Science and Technology 35(9), 171-180.
- 601 Kantachote, D., Torpee, S. and Umsakul, K. (2005) The potential use of anoxygenic phototrophic  
602 bacteria for treating latex rubber sheet wastewater. Electronic Journal of Biotechnology 8(3), 314-  
603 323.
- 604 Kim, M.K., Choi, K.-M., Yin, C.-R., Lee, K.-Y., Im, W.-T., Lim, J.H. and Lee, S.-T. (2004) Odorous swine  
605 wastewater treatment by purple non-sulfur bacteria, *Rhodopseudomonas palustris*, isolated from  
606 eutrophicated ponds. Biotechnology letters 26(10), 819-822.
- 607 Klamt, S., Grammel, H., Straube, R., Ghosh, R. and Gilles, E.D. (2008) Modeling the electron transport  
608 chain of purple non-sulfur bacteria. Mol Syst Biol 4, 156.
- 609 Klamt, S., Schuster, S. and Gilles, E.D. (2002) Calculability analysis in underdetermined metabolic  
610 networks illustrated by a model of the central metabolism in purple nonsulfur bacteria. Biotechnol  
611 Bioeng 77(7), 734-751.
- 612 Klein, G., Klipp, W., Jahn, A., Steinborn, B. and Oelze, J. (1991) The relationship of biomass,  
613 polysaccharide and H<sub>2</sub> formation in the wild-type and nifA/nifB mutants of *Rhodobacter capsulatus*.  
614 Archives of Microbiology 155(5), 477-482.
- 615 Koklu, H., Eroğlu, I.n., Gündüz, U., Yücel, M. and Türker, L. (2002) Aspects of the metabolism of  
616 hydrogen production by *Rhodobacter sphaeroides*. International Journal of Hydrogen Energy  
617 27(11), 1315-1329.
- 618 Lee, H.-S., Vermaas, W.F. and Rittmann, B.E. (2010) Biological hydrogen production: prospects and  
619 challenges. Trends Biotechnol 28(5), 262-271.
- 620 Li, X., Liu, T., Wu, Y., Zhao, G. and Zhou, Z. (2010) Derepressive effect of NH<sub>4</sub><sup>+</sup> on hydrogen  
621 production by deleting the glnA1 gene in *Rhodobacter sphaeroides*. Biotechnol Bioeng 106(4), 564-  
622 572.
- 623 Liang, C.-M., Hung, C.-H., Hsu, S.-C. and Yeh, I.-C. (2010) Purple nonsulfur bacteria diversity in  
624 activated sludge and its potential phosphorus-accumulating ability under different cultivation  
625 conditions. Applied Microbiology and Biotechnology 86(2), 709-719.
- 626 Madigan, M.T. and Gest, H. (1978) Growth of a photosynthetic bacterium anaerobically in darkness,  
627 supported by "oxidant-dependent" sugar fermentation. Archives of Microbiology 117(2), 119-122.

- 628 McKinlay, J.B. and Harwood, C.S. (2010a) Carbon dioxide fixation as a central redox cofactor  
629 recycling mechanism in bacteria. *Proceedings of the National Academy of Sciences of the United*  
630 *States of America* 107(26), 11669-11675.
- 631 McKinlay, J.B. and Harwood, C.S. (2010b) Carbon dioxide fixation as a central redox cofactor  
632 recycling mechanism in bacteria. *Proceedings of the National Academy of Sciences* 107(26), 11669-  
633 11675.
- 634 McKinlay, J.B. and Harwood, C.S. (2011) Calvin cycle flux, pathway constraints, and substrate  
635 oxidation state together determine the H<sub>2</sub> biofuel yield in photoheterotrophic bacteria. *MBio* 2(2),  
636 e00323-00310.
- 637 Melnicki, M.R., Eroglu, E. and Melis, A. (2009) Changes in hydrogen production and polymer  
638 accumulation upon sulfur-deprivation in purple photosynthetic bacteria. *International Journal of*  
639 *Hydrogen Energy* 34(15), 6157-6170.
- 640 Obeid, J., Magnin, J., Flaus, J., Adrot, O., Willison, J. and Zlatev, R. (2009) Modelling of hydrogen  
641 production in batch cultures of the photosynthetic bacterium *Rhodobacter capsulatus*. *International*  
642 *Journal of Hydrogen Energy* 34(1), 180-185.
- 643 Overmann, J. and Garcia-Pichel, F. (1998) The phototrophic way of life: The Prokaryotes: an evolving  
644 electronic resource for the microbiological community. M. Dworkin, New York, Springer.
- 645 Patton, C.J. and Truitt, E.P. (1992) Methods of Analysis by the US Geological Survey National Water  
646 Quality Laboratory: Determination of the Total Phosphorus by a Kjeldahl Digestion Method and an  
647 Automated Colorimetric Finish that Includes Dialysis, US Geological Survey.
- 648 Rodionov, Y.V., Lebedeva, N.V. and Kondratieva, E.N. (1986) Ammonia inhibition of nitrogenase  
649 activity in purple and green bacteria. *Archives of Microbiology* 143(4), 345-347.
- 650 Sarles, L.S. and Tabita, F.R. (1983) Derepression of the synthesis of D-ribulose 1, 5-bisphosphate  
651 carboxylase/oxygenase from *Rhodospirillum rubrum*. *J Bacteriol* 153(1), 458-464.
- 652 Schultz, J. and Weaver, P. (1982) Fermentation and anaerobic respiration by *Rhodospirillum rubrum*  
653 and *Rhodopseudomonas capsulata*. *J Bacteriol* 149(1), 181-190.
- 654 Seitz, H.J., Schink, B., Pfennig, N. and Conrad, R. (1990) Energetics of syntrophic ethanol oxidation in  
655 defined chemostat cocultures - 1. Energy requirement for H<sub>2</sub> production and H<sub>2</sub> oxidation. *Archives*  
656 *of Microbiology* 155(1), 82-88.
- 657 Szilveszter, S., Ráduly, B., Ábrahám, B., Lányi, S. and Niculae, D.R. (2010) Mathematical models for  
658 domestic biological wastewater treatment process. *Environmental Engineering and Management*  
659 *Journal* 9(5), 629-636.
- 660 Tait, S., Tamis, J., Edgerton, B. and Batstone, D.J. (2009) Anaerobic digestion of spent bedding from  
661 deep litter piggery housing. *Bioresource technology* 100(7), 2210-2218.
- 662 Tao, Y., He, Y., Wu, Y., Liu, F., Li, X., Zong, W. and Zhou, Z. (2008) Characteristics of a new  
663 photosynthetic bacterial strain for hydrogen production and its application in wastewater treatment.  
664 *International Journal of Hydrogen Energy* 33(3), 963-973.
- 665 Wang, X., Modak, H.V. and Tabita, F.R. (1993) Photolithoautotrophic growth and control of CO<sub>2</sub>  
666 fixation in *Rhodobacter sphaeroides* and *Rhodospirillum rubrum* in the absence of ribulose  
667 bisphosphate carboxylase-oxygenase. *J Bacteriol* 175(21), 7109-7114.
- 668 Yetis, M., Gündüz, U., Eroglu, I., Yücel, M. and Türker, L. (2000) Photoproduction of hydrogen from  
669 sugar refinery wastewater by *Rhodobacter sphaeroides* OU 001. *International Journal of Hydrogen*  
670 *Energy* 25(11), 1035-1041.
- 671 Zhu, H., Suzuki, T., Tsygankov, A.A., Asada, Y. and Miyake, J. (1999) Hydrogen production from tofu  
672 wastewater by *Rhodobacter sphaeroides* immobilized in agar gels. *International Journal of Hydrogen*  
673 *Energy* 24(4), 305-310.